North Carolina Agricultural and Technical State University

# Aggie Digital Collections and Scholarship

2014

# A Model Approach To Flux-Pinning Properties Of Yba2Cu3O7-Î´ Thin Film Vortex States Via Non-Superconducting Impurities

Jr Ronald Gamble
*North Carolina Agricultural and Technical State University*

## Recommended Citation

# A Model Approach to Flux-Pinning Properties of YBa$_2$Cu$_3$O$_{7-\delta}$ Thin Film Vortex States via Non-Superconducting Impurities

Ronald S. Gamble, Jr

North Carolina Agricultural & Technical State University

A thesis submitted to the graduate faculty

in partial fulfillment of the requirements for the degree of

MASTER OF SCIENCE

Department: Physics

Major: Physics

Major Professor: Dr. Abebe Kebede

Greensboro, North Carolina

2014

The Graduate School
North Carolina Agricultural and Technical State University
This is to certify that the Master's Thesis of


Ronald S. Gamble, Jr


has met the thesis requirements of
North Carolina Agricultural and Technical State University


Greensboro, North Carolina
2014


Approved by:


_____

Dr. Abebe Kebede
Major Professor, Advisor

_____

Dr. Dhananjay Kumar
Committee Member


_____

Dr. Ken Flurchick
Committee Member


_____

Dr. Abdellah Ahmidouch
Department Chair


_____

Dr. Sanjiv Sarin
Dean, The Graduate School

## *Biographical Sketch*

Born on March 21st, 1989 at Wright Patterson Air Force Base outside of Dayton, Ohio, Ronald S. Gamble JR the son of two parents each of whom have had careers in the STEM fields. Since an early age, he has always excelled in mathematics and the sciences, from taking apart his mother's computer as a child to now researching fundamental physical theories as an adult. But to compliment these left brain qualities Ronald is an experienced artist as well, having sold artwork across the U.S. and internationally in Italy. Rewarded for his accomplishments at North Carolina A&T State University in 2014, Ronald received the award for the 2013-2014 Outstanding Graduate Student of the Year for the College of Arts & Sciences.  Accompanied by a resume of accomplishments and grounded by his strong religious faith, he is determined and personally tasked to help educate and to study the laws of nature that govern the physical phenomena that captures his curiosity.

### *Dedication*

To my family and mother, for the faith and determination you've given me.

## *Para El Benificio Del Mundo*

*(For The Benefit of the World)*

## *Acknowledgements*

To my advisor of six years Dr. Abebe Kebede, the Physics department and all who have helped me achieve my successes thus far.

# Table of Contents

# List of Figures

# List of Tables

# Abstract

Thin film $YBa_2Cu_3O_{7-\delta}$ (YBCO) samples with added non-superconducting nanodot defects of $CeO_2$ and $BaSnO_2$ are the focus of recent high-temperature superconductor studies. These nanodots allow magnetic flux $(\boldsymbol{\phi_B})$ to penetrate at these sites of the superconducting lattice, thus creating a magnetic flux vortex state. Examining the structure shows that these quantized magnetic flux vortices arrange themselves in a self-assembled lattice. The nanodots, with non-superconducting properties, serve to present structural properties to restrict motion of these vorticies under a *pinning-force* and to enhance the critical current density. A formulation of a new model for the system by a variation in the electron pair velocity via the virtual work from the nanodot defects in accordance to the well-known Superconductivity theories is tested. A solution to the expression for the magnetic flux, zero net force and pair velocity will generate a setting for the optimal deposition parameters of number density, growth geometry and mass density of these nanodot structures. With a calculation of pair velocities from a similar work, a comparison is made between experimental and theoretical velocity calculations using growth geometry and chemical potential. This will yield insight into how the current density for a doped high-temperature superconductor will be modified and tuned based on the dynamics and density of the nanodots themselves.

# CHAPTER 1

# Introduction

Superconductivity has been at the forefront of solid state physics and materials science research. The electronic applications possible from this phenomenon are near endless, along with other applications to aid in the research of other physical disciplines (gravitation, quantum mechanics, accelerator physics, etc.). Thus, the motivation of this study is to contribute to the overall understanding of this phenomenon.

## 1.1 The Superconducting State

Superconductivity is the homogenous ordering of the conduction electrons in their respective planes within the lattice of a metal, alloy or similarly structured material. Electrical resistivity of the material drops to nearly zero when the material is cooled to an effectively low temperature ($< 77K$) triggering a phase transition in the material. At this critical temperature, the material undergoes a transition from a Normal phase with finite electrical resistivity in the material to a superconducting state with zero electrical resistivity. Within this highly ordered state establishment of loosely paired conducting electrons or Cooper Pairs arise. These associated pairs of electrons are only ordered at or below the *critical temperature* $(T_c)$ of the material, an increase of the temperature (above this transition temperature) will cause theses pairs to become disordered increasing their respective entropy of the system due to heat and depair. A significantly strong applied magnetic field will destroy superconductivity if the value is above the critical field limit of $\mathbf{H_c(T)}$ as a function of temperature. At the phase transition temperature or critical temperature the critical field limit is zero [1], $\mathbf{H_c(T)} = 0$.

Meissner and Ochsenfeld [1] (1953) found that if a superconductor is cooled in a magnetic field to a temperature below the transition temperature $\boldsymbol{T_c}$ the superconducting material will expel all magnetic

lines of flux [1]. Thus, superconductivity is characterized by the Meissner effect, a complete ejection of magnetic flux lines during its transition to the superconducting state figure (1); decreasing the interior magnetic field but also increasing the exterior magnetic field of the superconductor.
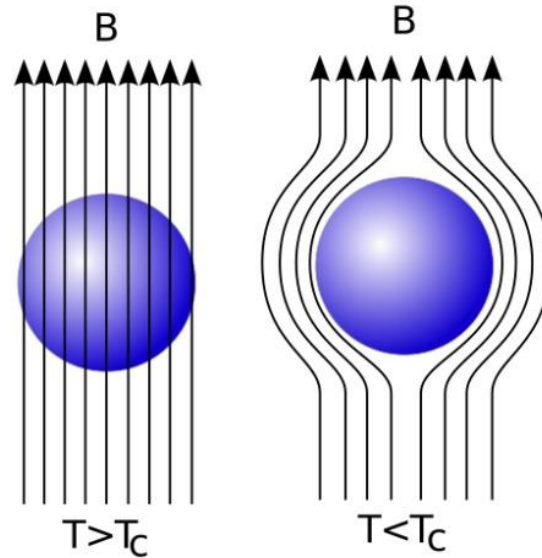


**Figure 1 Meissner effect during superconductivity** [2], [1]

Constricting samples to elongated thin planes of material with the long axes (**c**) parallel to the applied magnetic field, $\mathbf{B_a}$ . Now the demagnetizing field contribution to the interior magnetic field $B$ is expressed in equation (1.1) or in terms of the magnetization over the applied field of the sample as expressed in equation (1.2):

$$B \;=\; B_a + \; 4\pi M \;=\; 0 \qquad\qquad\text{(eqn. 1.1)}$$

$$M/B_a \;=\; -1/4\pi \qquad\qquad\text{(eqn.1.2)}$$

The result $\mathbf{B} = 0$ cannot be derived from the characterization of a superconductor as a medium of zero resistivity$(\rho)$. From Ohm's Law, $\mathbf{E} = \rho\mathbf{J}$, it's seen that if the resistivity $\boldsymbol{\rho}$ goes to zero while $\boldsymbol{J}$ is held finite, then $\mathbf{E}$ must be zero. On the other hand, a Maxwell equation $\frac{d\mathbf{B}}{dt}$ is proportional to the curl of the

electric field **E**; $\frac{d\mathbf{B}}{dt} \propto \nabla \times \mathbf{E}$ so that zero resistivity implies $\frac{d\mathbf{B}}{dt} = 0$ but not **B** = 0. This shows that the Meissner effect is a vital attribute of superconductivity [1]. But one cannot simply characterize the magnetic field induction in the superconducting state of Type-II superconductors in this way due to the duality of Normal and Superconducting states.

## 1.2 London Theory

Formulation of an expanded description of the Meissner effect is needed. In 1953, Fritz and Hans London, promoted a phenomenological theory which allowed them to justify the exotic electromagnetic properties of many superconducting materials. In particular, they were able to account for the existence of persistent currents and the exclusion of magnetic flux from the interior of a superconductor. The London equations suggest that two be modifications to Maxwell's equations in order to describe the electromagnetic properties of superconductors. Equations (1.3 and 1.4) express this in terms of the time derivative of the electric current density [2; 3].

$$\boldsymbol{E} = \frac{4\pi\lambda^2}{c^2} \frac{d\boldsymbol{J}}{d\boldsymbol{t}} = \frac{m_*}{n_* e_*^2} \frac{d\boldsymbol{J}}{d\boldsymbol{t}} \qquad \text{(eqn.1.3)}$$

$$\boldsymbol{B} = -\frac{m_*}{n_* e_*^2} \nabla \times \boldsymbol{J_s} \qquad \text{(eqn.1.4)}$$

Here *E and B* are the internal electric and magnetic fields respectively, *J* is the current density of the superconducting electrons, and $n_*, m_*$ *and* $e_*$ are the number density of charge carriers, the mass of superconducting electron pairs and the charge associated with electrons. The Meissner effect implies a magnetic susceptibility $\boldsymbol{\chi} = -1$. The London equations manipulate Ohm's Law of electrical conductivity in the normal state to describe conductivity in the superconducting state. Equation 1.3 expresses the Lorentz Force uniformly for all electrons in the superconducting state, a recasting of Newton's second Law of Motion. Equation 1.4 on the other hand needs more rationale to be an effective expression for the

superconducting state. In the superconducting state the current density is directly proportional to the vector potential **A** of the local magnetic field. Using Faraday's Law of Electromagnetic Induction as the curl of the electric field $\mathbf{\nabla} \times \mathbf{E} = -\frac{1}{c}\left(\frac{d\mathbf{B}}{dt}\right)$, the following result is obtained [2]:

$$\frac{\partial}{\partial t}\left(\nabla \times J + \frac{n_* e_*{}^2}{m_* c} B\right) = 0 \qquad \text{(eqn.1.5)}$$

Equation (1.5) allows for both constant and exponentially decaying solutions. The London brothers recognized this from Meissner effect that constant nonzero solutions were not physical and further postulated that not only was the time derivative of equation (1.5) equal to zero, but also that the expression in the parenthesis must be exactly zero [2]. The results from these two postulates for additional variations to Maxwell's Equations for the handling of electromagnetic phenomena in the superconducting state are the London Equations. The London Equations are now able to be expressed in terms of the magnetic vector potential and the local magnetic field.

$$J = \frac{-1}{\mu_0 \lambda_L^2} A \qquad \text{(eqn.1.6)}$$

$$\nabla \times J = \frac{-1}{\mu_0 \lambda_L^2} B \qquad \text{(eqn.1.7)}$$

Independent of geometry and in the London gauge $[\mathbf{\nabla} \cdot \mathbf{A} = 0]$, the curl of the current density and the Lapacian operator of the magnetic field gives the description of the Meissner effect in terms of the magnetic field penetration depth $\lambda$ in the superconducting state.

Under static conditions,

$$\nabla \times (\nabla \times B) = -\nabla^2 B = \mu_0 \nabla \times J \qquad \text{(eqn.1.8)}$$

$$\nabla^2 B = \frac{B}{\lambda_L^2} \qquad \text{(eqn.1.9)}$$

Further analysis of this leads to the solution of [1]

$$\mathbf{B}\left(\chi\right) \; = \; \mathbf{B}\left(0\right)e^{-\chi/\lambda_L} \qquad\qquad \text{(eqn.1.10)}$$

Describing the magnetic field penetration as it exponentially decays further into the superconducting material. The solution to equation (1.8) accounts for the Meissner effect in the superconducting state, this equation does not allow a solution in uniform space implying why there is no uniform magnetic field in a superconductor. $\mathbf{B}(\mathrm{r}) \; = \; \mathbf{B}_0 \; = \;$ Const. is not a valid solution unless $\mathbf{B}(\mathrm{r}) \; = \; \mathbf{B}_0 \; = \; 0$. The result follows because $\nabla^2 \mathbf{B} \; = \; 0$ is always zero but $\frac{\mathbf{B}}{\lambda^2}$ is not zero unless $\mathbf{B}_0 \; = \; 0$. For the Cooper Pairs of mass $(m_*)$, charge $(e_*)$ and number density $(n_*)$ the London Penetration Depth, $\lambda_L$, is

$$\lambda_L = \sqrt{\frac{\epsilon_0 m_* c^2}{n_* e_*^2}} \qquad\qquad \text{(eqn.1.11)}$$

In thin film samples, the Meissner effect is not complete due to the thickness of the sample. It follows that the critical field $\mathbf{H_c}$ of thin films in parallel magnetic fields will be very high. Thus, in thin film superconductors the London Equations are local equations at a single point in the thin film with $\mathbf{J}(\mathrm{r})$ and $\mathbf{A}(\mathrm{r})$, the current density and magnetic vector potential respectively [1]. A very important parameter to include is the Coherence Length, which is a measure of the range over the average $\mathbf{A}(\mathrm{r})$ to obtain $\mathbf{J}(\mathrm{r})$ for time $(\mathbf{t})$. The coherence length measures this range as a distance in which the superconducting electron concentration cannot change drastically in a spatially-varying magnetic field. It is also a measure of the minimum spatial extent of a transition layer between the normal and superconductor layers. Any spatial variation in the state of an electronic system requires extra kinetic energy. A modulation of the eigenfunction of the kinetic energy will increase the integral of $\frac{d^2 \varphi}{dx^2}$. It is reasonable to restrict the spatial variation of $\mathbf{J}(r)$ in such a way that the extra energy is less than the stabilization energy of the superconducting state. Comparing the plane wave $(\psi(x))$ with the modulated wave-function $(\phi(x))$ [1]:

$$\psi(x) = \; e^{-ikx} \qquad\qquad \text{(eqn.1.12)}$$

$$\phi(x) = \frac{1}{\sqrt{2}}(e^{i(k+q)x} + e^{ikx}) \tag{eqn.1.13}$$

The probability density associated with the plane wave is uniform in space,

$$\psi^*(x)\psi(x) = e^{-ikx}e^{ikx} = 1 \tag{eqn.1.14}$$

Whereas $\phi^*(\mathbf{x})\phi(\mathbf{x})$ is modulated with the wave vector $\mathbf{q}$;

$$\phi^*(x)\phi(x) = \frac{1}{2}(e^{i(k+q)x} + e^{ikx})(e^{i(k+q)x} + e^{-ikx}) \tag{eqn.1.15}$$

$$= \frac{1}{2}(2 + e^{iqx} + e^{-iqx}) = 1 + Cos(qx) \tag{eqn.1.16}$$

The kinetic energy of the wave $\psi(\mathbf{x})$ is:

$$\varepsilon = \frac{\hbar^2 k^2}{2m} \tag{eqn.1.17}$$

The kinetic energy of the modulated density distribution is higher for,

$$\int dx \, \phi^* \left( -\frac{\hbar^2}{2m}\frac{d^2}{dx^2} \right) \phi \tag{eqn.1.18}$$

$$= \frac{1}{2}\left(\frac{\hbar^2}{2m}\right)[(k+q)^2 + k^2] \cong \frac{\hbar^2}{2m}k^2 + \frac{\hbar^2}{2m}kq \tag{eqn.1.19}$$

Where the $q^2$ term is neglected because $q \ll k$ [1], the increase of energy required to modulate is $\left(\frac{\hbar^2 kq}{2m}\right)$.

If this increase exceeds the energy gap ($E_g$), superconductivity will be destroyed. The critical value ($\mathbf{q}_0$) of the modulation wave vector is given by

$$\frac{\hbar^2}{2m}k_F q_0 = E_g \tag{eqn.1.20}$$

We define an intrinsic Coherence Length ($\xi_0$) related to the critical modulation by

$$\xi = \frac{1}{q_0} \qquad \text{(eqn.1.21)}$$

$$\xi = \frac{\hbar^2 K_F}{2mE_g} = \frac{\hbar v_F}{2E_g} \qquad \text{(eqn1.22)}$$

, Where $v_F$ is the electron velocity at the Fermi surface. On BCS Theory, a similar result is obtained [1]:

$$\xi_0 = \frac{2\hbar v_F}{\pi E_g} \qquad \text{(eqn.1.23)}$$

The Coherence length ($\xi_0$) and the London Penetration Depth ($\lambda_L$) depend on the mean-free path of the electrons (L) measured in the Normal state. When there are nanodots in the superconductor, the mean-free path of the electrons is reduced. The coherence length can be approximated as such:

$$\xi \approx \sqrt{\xi_0 L} \qquad \text{(eqn.1.24)}$$

And

$$\lambda \approx \lambda_L \sqrt{\frac{\xi_0}{L}} \qquad \text{(eqn.1.25)}$$

$$\frac{\lambda}{\xi_0} \approx \frac{\lambda_L}{L} \qquad \text{(eqn.1.26)}$$

## 1.3 BCS Theory of Superconductivity

BCS Theory is the basis of a quantum mechanical formulation of superconductivity first theorized by Bardeen, Cooper, and Schrieffer in 1957. There exists a "BCS wave function" composed of particle pairs ($\kappa \uparrow \; and - \kappa \downarrow$) which, when treated by the BCS theory, gives the formal electronic superconductivity observed in materials and exhibits the energy gaps expressed in equation (1.20). This energy gap can be

applied to (*d-wave)* particle pairing in type-II superconductors, YBCO in this case. There is a set of criterion that the BCS theory assumes [4], [1], [5]:

1. An attractive interaction between electrons can lead to a ground state separated from the excited states by an energy gap ($E_g$). The critical field, the thermal properties and most of the electromagnetic properties are consequences of this energy gap.

2. The electron-lattice-electron interaction (or electron-phonon interaction) leads to an energy gap of the observed magnitude. The indirect interaction proceeds when one electron interacts with the lattice and deforms it: a second electron sees the deformed lattice and adjusts itself to take advantage of the deformation to lower its current energy state. Thus, the second electron interacts with the first electron by way of the lattice deformation.

3. The penetration depth and the coherence length emerge as natural consequences of the BCS theory. The London equations are obtained for magnetic fields that spatially vary slowly. Thus, the central phenomenon in the superconducting state, the Meissner effect, is obtained by natural means.

4. The criterion for the transition temperature of a superconducting material involves the electron orbital density ($D(\epsilon_F)$) of one spin at the Fermi level and the electron-lattice interaction $U$, which can be estimated from the electrical resistivity because the resistivity at room temperature is a measure of the electron-phonon interaction. For $UD(\epsilon_F) \ll 1$ the BCS theory predicts

$$T_c = 1.14\theta e^{-\frac{1}{UD(\epsilon_F)}}$$ 
(eqn.1.27)

   Where $\theta$ is the Debye temperature and $U$ is an attractive interaction. The result for $T_c$ is satisfied at least qualitatively by experimental data. There is an interesting apparent paradox: the higher the resistivity at room temperature the higher $U$, and the higher $T_c$ is.

5. Magnetic flux through a superconducting ring or hole-doped normal state defect for thin film samples is quantized and the effective unit of charge is 2*e* rather than *e*. The BCS ground state

involves pairs of electrons, thus the quantization in terms of the pair charge $2e$ is a consequence of the theory. [1]

The BCS theory is then formulated from the use of an interaction potential in the form of [6]:

$$\mathcal{H} = \mathcal{H}_{KE} + \mathcal{H}_V \qquad \text{(eqn.1.28)}$$

Where $\mathcal{H}_V = \mathcal{H}_V^{(0)} + \mathcal{H}_V^{(1)}$ is the interaction potential and the variation of the interaction, respectively.

$$\mathcal{H}_{KE} = \sum_{k\sigma} \epsilon_k C_{k\sigma}^\dagger C_{k\sigma} \equiv \sum_{k\sigma} \epsilon_k \hat{n}_{k\sigma} \qquad \text{(eqn.1.29)}$$

Where $\hat{n}_{k\sigma}$ is the number of fermions in that state and $C_{k\sigma}^\dagger C_{k\sigma}$ are the creation-annihilation operators for the fermionic interaction. This Hamiltonian for the kinetic energy is more simply minimizing $\mathcal{H} - \mu \hat{N}$, where $\hat{N}$ is the total number and $\mu$ is the chemical potential. Conventionally, the energy scale has been shifted so that $\mu = 0$ and $\epsilon_k$ is the Fermi energy at $T = 0$ from the chemical potential. Now the interaction energy can be written as [5], [6], [7]:

$$\mathcal{H}_V^{(0)} = \sum_{pkk'} V_{kk'}^{(0,p)} \sum_{\sigma 1,\sigma 2} \left( C_{k'+\frac{p}{2},\sigma 1}^\dagger C_{-k'+\frac{p}{2},\sigma 2}^\dagger C_{k+\frac{p}{2},\sigma 1} \right) \qquad \text{(eqn.1.30)}$$

Where $V_{kk'}^{(0,p)} = -V_{k,-k'}^{(0,p)}$ ensures the singlet symmetry and the triplet term of the interaction potential [5] is

$$\mathcal{H}_V^{(1)} = \sum_{pkk'} V_{kk'}^{(1,p)} \left( C_{k'+\frac{p}{2},\sigma 1}^\dagger \boldsymbol{\tau}_{\sigma_1',\sigma_2'} C_{-k'+\frac{p}{2},\sigma_2'}^\dagger \right) \cdot \left( C_{k+\frac{p}{2},\sigma_1} \boldsymbol{\tau}_{\sigma_1,\sigma_2} C_{k+\frac{p}{2},\sigma_2} \right) \qquad \text{(eqn.1.31)}$$

An effective Hamiltonian for this interaction can arise from a unitary transformation formulated by Theoretical Physicist and Mathematician Nikolay Bogolyubov. The Bogolyubov Transformation (Bogo Transformation) consists of a unitary transformation of the canonical anticommutation relation to another unitary relation via isomorphisms of the commutation relation algebra. The use of this addition to the BCS Theory will produce a set of solutions that describe the effective Hamiltonian and quasiparticle creation through fermionic particle pairing of electrons [5].

$$\mathcal{H}_{pair}^{eff} \approx -\sum_{k}\left(\Delta_{k}^{*}C_{-k\downarrow}C_{k\uparrow} + \Delta_{k}C_{k\uparrow}^{\dagger}C_{-k\downarrow}^{\dagger}\right) \tag{eqn.1.32}$$

Where

$$\Delta_{k} \equiv -\sum_{k'}V_{kk'}^{(0)}\langle C_{-k'\downarrow}C_{k'\uparrow}\rangle$$

This transformation will only give an effective Hamiltonian and pair Hamiltonian for the superconducting phase only below the lower critical field limit ($H_{c1}$). Type-I & type-II superconductors can be considered to share a likeness in their conductive and thermodynamic properties within this field limit and thus can be treated as if they are homogenous in nature. In type-II superconductors there exists a "*Vortex state*" that of which lies between the lower critical field ($H_{c1}$) and the upper critical field ($H_{c2}$) where this effective Hamiltonian solution does not exist, suggesting an unknown set of solutions to the BCS Theory involving the Vortex State of type-II superconductors (YBCO in this case). From here there isn't enough evidence to suggest that the BCS Theory of superconductivity on the microscopic scale is a sufficient theory to formulate a description for type-II superconductors, especially thin film samples.

## 1.4 Ginzburg-Landau Free-Energy

The Ginzburg-Landau free energy theory is the macroscopic elastic description appropriate for any superconductor [8]. The use of the Ginzburg-Landau free energy approach to describe macroscopic phenomena in superconductivity is focused towards a more general theory of the superconducting state without the inclusion of most of the microscopic phenomenological happenings in that state. Unlike the BCS theory that takes on the dynamics of the quasiparticle pairing (creation and annihilation of Cooper Pairs from interacting superconducting electrons), Ginzburg and Landau's formulation is a field

methodology. Using the superconducting field parameters like that of $\Psi(r)$, the Ordering parameter which is allowed to have complex values, and the magnetic vector potential $A(r)$ of which can only have real values due to its physical nature of the vector field. Note that although this is a "field approach" the magnetic vector potential in this case is a 3-component parameter with the usual gauge freedoms [8]. Venturing deeper into this description, thermodynamic properties of the state must arise in the form of the free-energy generated by the magnetic fields in the superconducting state giving the Ginzburg-Landau equation for the free-energy density of the system [5], [3], [9]:

$$F_{GL}(r) = F_{grad}(r) + F_L(|\Psi(r)|) + U_{mag}(B(r)) \qquad \text{(eqn.1.33)}$$

Where $F_{GL}(r)$ is the free-energy density of the system in terms of the Landau term for the order parameter $|\Psi|$, the gradient term $F_{grad}(r)$ which includes the magnetic vector potential and the gradient of the order parameter. The magnetic field energy term is the usual potential energy associated with magnetostatics [8]. According to these parameters formulated by Ginzburg and Landau, along with the coherence length and penetration depth (also with Ginzburg-Landau parameters), characterization of the type-II superconductor can be achieved. Penetration depth and coherence length in terms of Ginzburg-Landau theory can very much be applied to describe the layered dynamics of thin film superconductors like that of YBCO. The importance of Ginzburg-Landau theory is to provide a foundation for a uniform macroscopic approach to type-II superconductivity, with this one can begin to convey a theory that describes the superconducting phase in type-II materials, excluding the Vortex state of added nanodots to the materials via nanodot deposition.

## 1.5  High Temperature Superconductivity

High temperature superconductivity is characterized from the coherence length, penetration depth, meissner effect and the Vortex state between the lower and upper critical field limits. Also referred to as type-II superconductors, their complete properties are still yet unknown to Experimentalist and even Theoretical Physicists within the field of Solid State Physics. Because of their "exotic" superconducting nature, it is very difficult to pinpoint their exact magnetic field limits within the vortex state. Intrinsic properties of type-II materials is that the ratio of the penetration depth to coherence length $(\lambda/\xi)$ along with their applied magnetic field response. Figure (2) illustrates this field response, the magnetization as a function of an applied magnetic field.
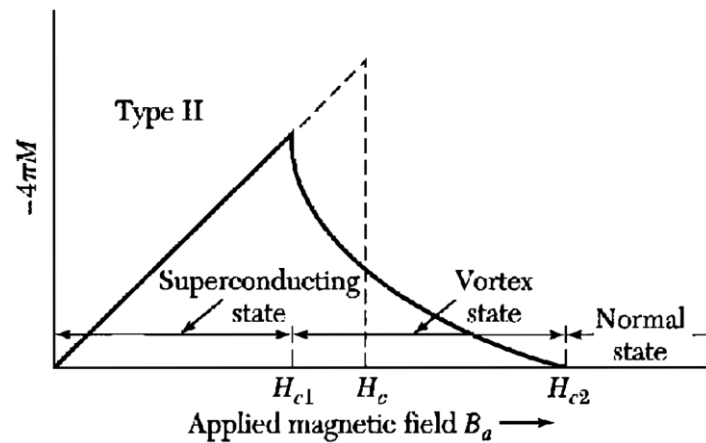


**Figure 2: Magnetization (M) as a function of applied magnetic field (B) for type-II superconductors** [1]

The importance of type-II materials is the critical current density $(J_c)$ and their critical temperature $(T_c)$, for YBCO $T_c \cong 90K$. With such high critical temperatures type-II materials show much promise in their current and future applications having the ability to superconduct at high temperatures to work with, broadening our scope of contemporary technologies.

# CHAPTER 2

## Heteroepitaxial Growth of Microstructure

### 2.1  Pulsed Laser Deposition

The Pulsed Laser Deposition is a well-known growth technique for the creation of thin film samples [8], [9], [10]. Using an Excrimer Krypton Fluoride (KrF) laser with a 248nm wavelength thin film samples of $YBa_2Cu_3O_{7-\delta}$ (YBCO) were deposited onto $LaAlO_3$ substrates. The laser deposition process involves the firing of the KrF laser at a YBCO target pellet creating a plasma plume of the material (laser ablation) with certain angular distribution and dispersion velocity as shown in figure (3), with the laser deposition assembly shown in figure (4).



Krypton Fluoride-YBCO laser plume

Vacuum Chamber
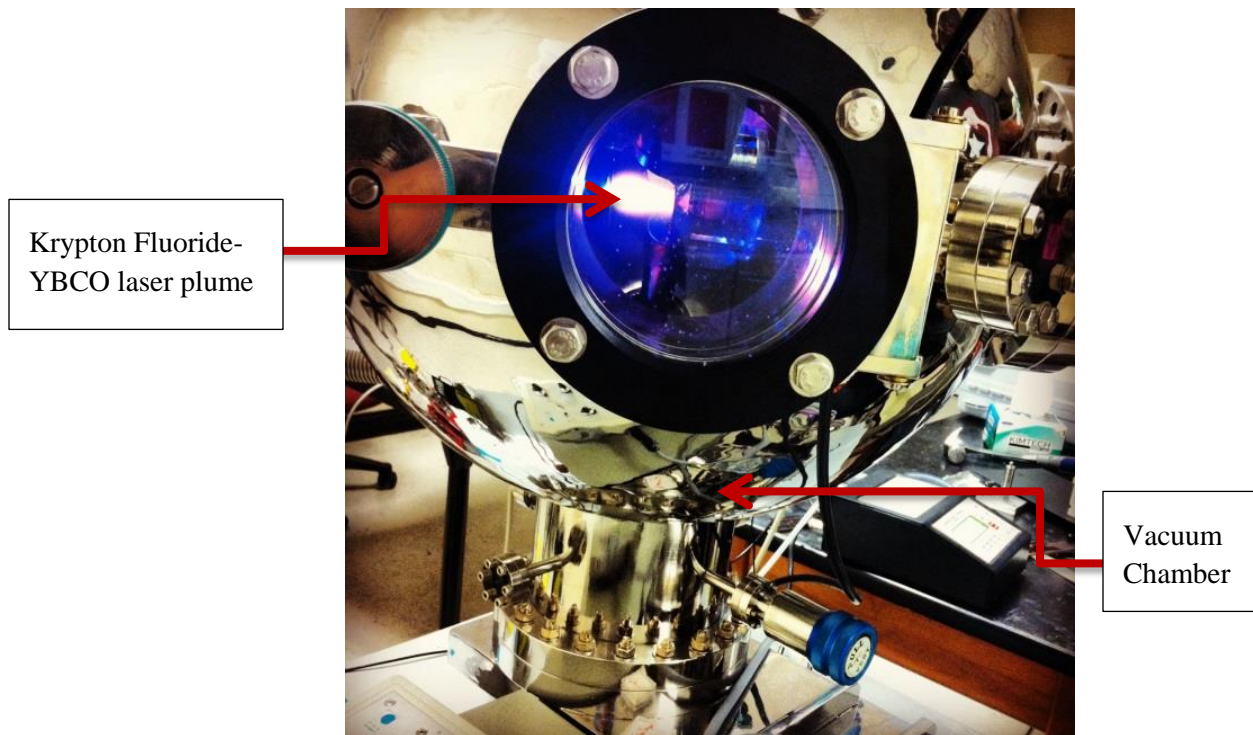
**Figure 1: Pulsed Laser Deposition of YBCO thin film**
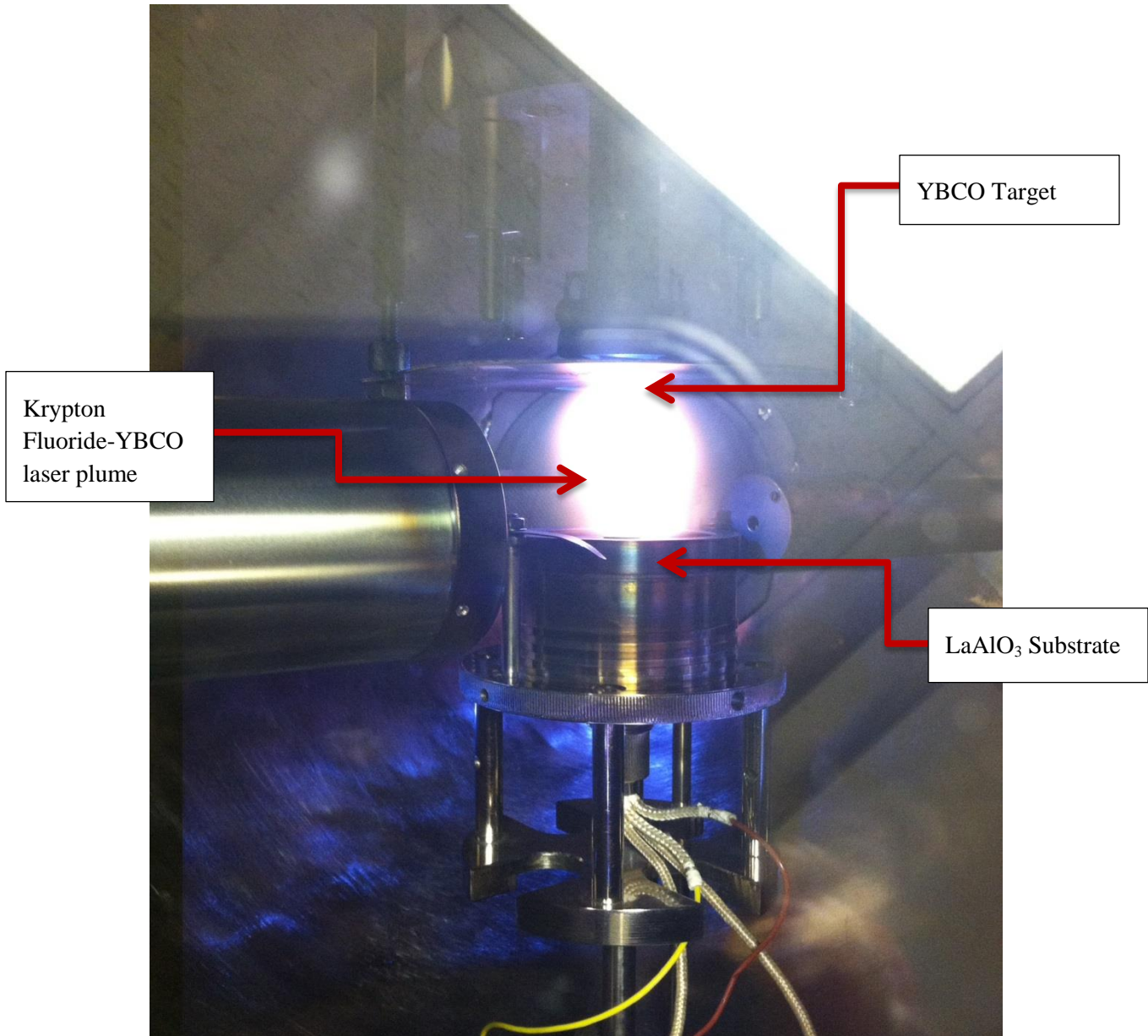
**Figure 2: Pulsed Laser Deposition substrate and target assembly during deposition of YBCO on to the LaAlO$_3$ substrate**

This plasma plume will deposit onto the substrate previously heated to an experimental standard of $\sim760 \pm 10\ ℃$, the ablation process requires a constant oxygen pressure about 300 mTorr to induce an increase in the Copper-Oxide (CuO) sites in the structure of the sample effecting the stoichiometry of the thin film. Table 2.1 shows the deposition parameters for each thin film sample created using the PLD

technique. A common factor in each of the samples created is the Oxygen pressure, a very important parameter during the ablation of the target to the thin film substrate.

**Table 1 Pulsed Laser Depostion Parameters**

| Deposition Date | Vacuum Pressure | Substrate Temperature | $O_2$ Pressure | Beam Energy | # of Pulses | Pulse Rate | $O_2$ Flood Pressure |
|---|---|---|---|---|---|---|---|
| 11/25/13 | 9.3 µTorr | 786 $^0$C | 300 mTorr | 550 mJ | YBCO: 20,000 CeO$_2$:20 | 10hz | |
| 12/2/13 | 9.3 µTorr | 775 $^0$C | 300 mTorr | 550 mJ | YBCO: 20,000 BaSnO$_3$:20 | 10hz | |
| 2/20/14 | 1.7 µTorr | 775 $^0$C | 203 mTorr | 500 mJ | YBCO: 10,000 CeO$_2$: 30 | 5hz | 5.08 Torr |
| 2/24/14 | 5.3 µTorr | 775 $^0$C | 200 mTorr | 500 mJ | 10,000 | 5hz | 335 Torr |
| 3/5/14 | 1.4 µTorr | 778$^0$C | 205 mTorr | 400 mJ | 15,000 | 10hz | 300 Torr |

**Krypton Fluoride (KrF) Laser:**

- 248 nm wavelength
- 20-35 ns pulse duration
- Laser wavelength is proportional to film penetration depth at surface (120 nm in the AxB plane and 800 nm in the C plane)
- Laser fluence at the surface ranges from 1-3 j/cm2

**Plasma Plume:**

- Plasma plume density is pertinent to the stoichiometry of the sample —-for all species—expand with identical angular distributions
- Optimum growth rate should float around 1 angstrom per pulse

**Stoichiometry:**

- Laser irradiation before deposition (pre-ablation) is necessary (for materials like that of ceramics) to establish a "steady state" resulting in the enrichment of the target surface of the less-volatile component
- Concentration of the target components are formulized from the angle and rotational velocity of the laser

**Film Thickness:**

- Film thickness is directly affected by the heating temperature and the lateral positioning of the substrate on the heater
- Positioning from 0 – 4 cm on substrate heater with temperature gradient of 800-600 $^0$C resulting in an approximate ~450-280 nm sample thickness
- Laser beam energy effects the sample thickness
- The number of pulses and pulse duration affect the sample thickness

## 2.2  YBCO Thin Films

The crystalline compound YBa$_2$Cu$_3$O$_{7-\delta}$, Yttrium Barium Copper Oxide is synthesized by heating a combination of the metal carbonates between the temperatures of 1000 to 1300 K:

$$4BaCO_3 + Y_2(CO_3)_3 + 6CuO_3 + \left(\frac{1}{2} - \delta\right)O_2 \rightarrow 2YBa_2Cu_3O_{7-\delta} + 13CO_2$$
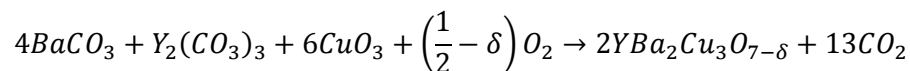
Modern synthesis of YBCO utilizes corresponding oxides and nitrates to synthesize the compound. In the normal state of YBCO it acts as a ceramic with high resistivity, but when YBCO is cooled down to its respective critical temperature (92K) and under goes a phase transition at that temperature; YBCO becomes superconducting. The superconducting properties of YBCO are at the mercy of its oxygen content, the value of $\delta$. Only compounds with oxygen content between $0 \leq x \leq 0.65$ become superconducting below the critical temperature (T$_C$), but when $x \sim 0.07$ YBCO superconducts at its highest temperature of 95K, or in the highest magnetic fields of 120T for **B** perpendicular and 250T for **B** parallel to the CuO$_2$ planes within the lattice of YBCO. Figure (5) illustrates the YBCO lattice structure for **a**, **b**, and **c** directional axes.

.
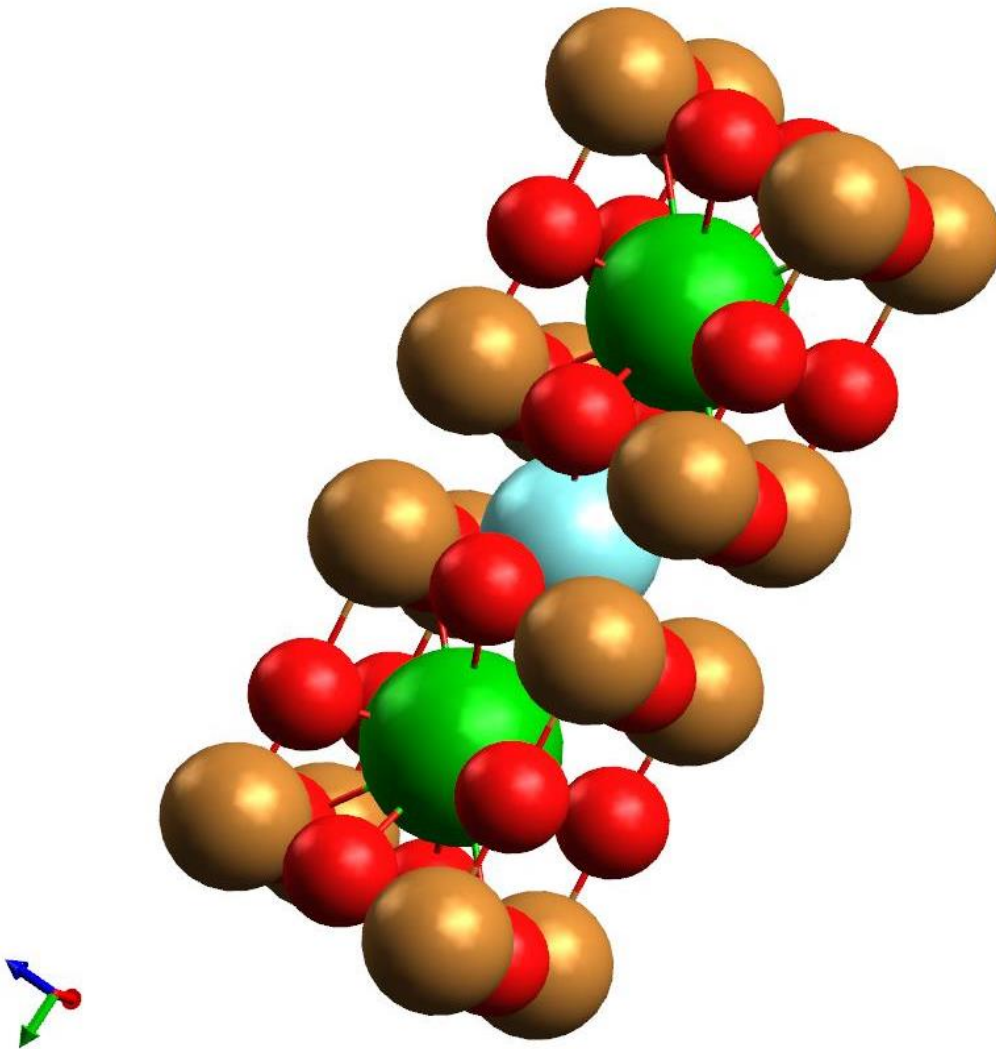


**Figure 3: YBCO Lattice Structure.**

**Blue: Yttrium**

**Green: Barium**

**Gold: Copper**

**Red: Oxygen**

One can see that within the structure of the YBCO lattice there are *planes*, these Copper-Oxide planes carry the conducting electrons within the lattice. When YBCO is in the superconducting phase, these planes become the source of the superconducting electron pairs. Modification to YBCO thin films have become a standard method in the study of its superconducting properties through the deposition of

nanodots to the lattice of YBCO [8], [9]. Deposition of these nanodots introduce normal state islands onto the thin film sample, and when in the presence of an applied magnetic field, these normal zones allow magnetic field lines to penetrate through the thin film thus creating magnetic flux and inducing an electrical current. The supercurrents circulating around these normal zones create magnetic flux vortices and optimizing superconductivity via an increase in the critical current density of the sample. In figures, (6) and (7) are the lattice structures of the nanodots, $CeO_2$ and $BaSnO_3$:
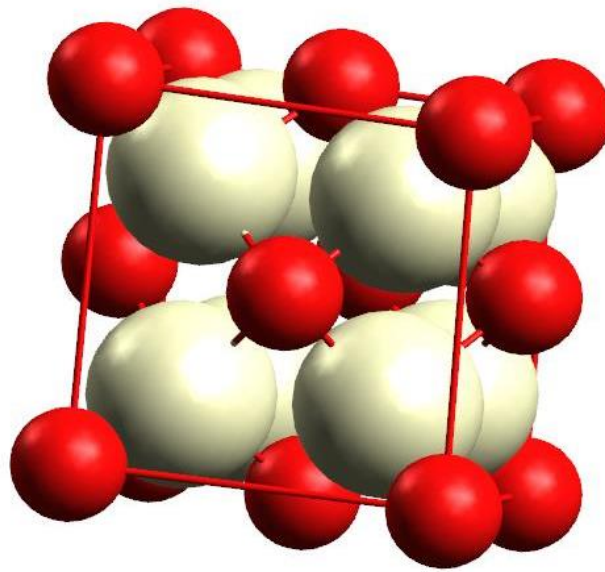


**Figure 4: CeO$_2$ Lattice Structure**
**White: Cerium**
**Red: Oxygen**
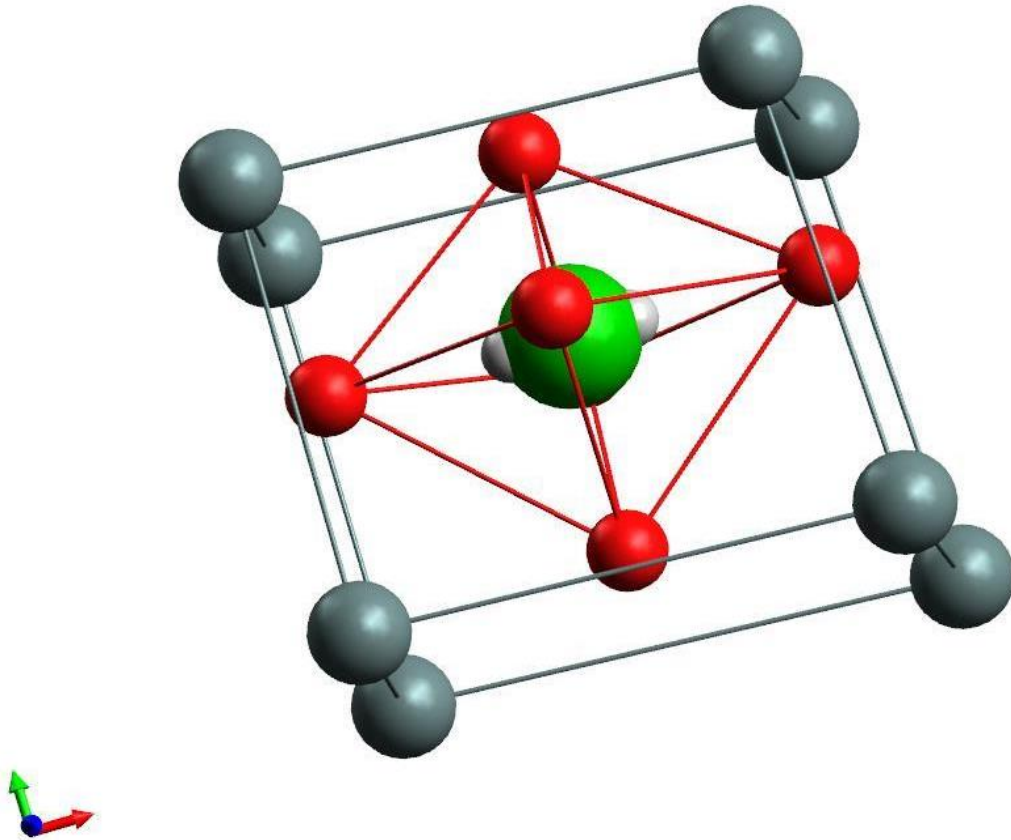
**Figure 5: BaSnO$_3$ Lattice Structure**
**Green: Tin**
**Gray:**
**Barium Red: Oxygen**

Using a control or default sample, measuring the magnetic moment and temperature of the sample gives the superconducting critical temperature of (~68.84 K) at a relatively zero magnetic moment (6.927 x 10$^{-12}$ A·m$^2$). This measurement, in figure (8), is made to show a typical result of YBCO in the superconducting state as it transitions to the normal state.
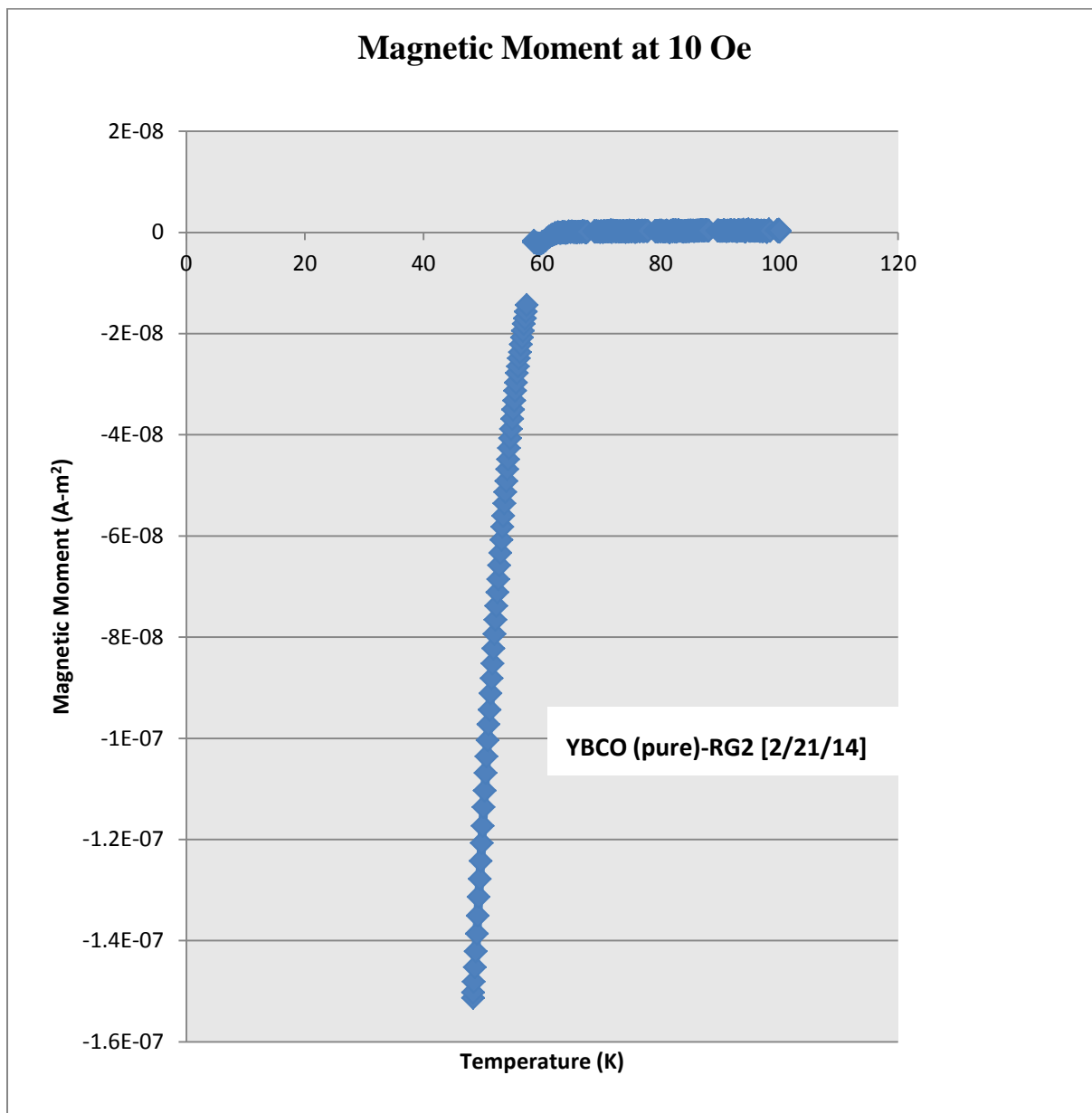
**Figure 6: Magnetic Moment vs Temperature for the sample RG2-YBCO(pure)[2/21/14] with an applied magnetic field strength of 10 Oe**

# CHAPTER 3

# Critical Current Density of YBCO Thin Films

## 3.1 Overview of Magnetic Flux and Critical Current Distributions

It is well known that any magnetic flux through a ring of supercurrent will become quantized and thus creating a magnetic flux vortex from the circulating supercurrents. As stated above, the normal zones of Barium Tin Oxide ($BaSnO_3$) and Cerium Oxide ($CeO_2$) deposited onto the thin film samples through laser ablation serve as field penetration sites inviting this magnetic flux through the sample. The creation of these magnetic flux vortices puts the YBCO sample in the vortex state, existing between the lower and upper critical field limits where $H_{c1} < H_{vortex} < H_{c2}$. The Vortex state of YBCO follows the Abrikosov Vortex lattice theory for the anisotropic surfaces of type-II superconductors [6]. The vortex structure is described by the Bessel function formulation of the magnetic field far from the core of the vortex and at $r \rightarrow 0$, respectively. At the coherence length$(\xi)$ [8],

$$\boldsymbol{B(r)} = \frac{\Phi_0}{2\pi\lambda_L^2} K_0(z) \left(\frac{r}{\lambda_L}\right) \approx \sqrt{\frac{\lambda}{r}} e^{\left(-\frac{r}{\lambda}\right)} \qquad \text{(eqn.3.1)}$$
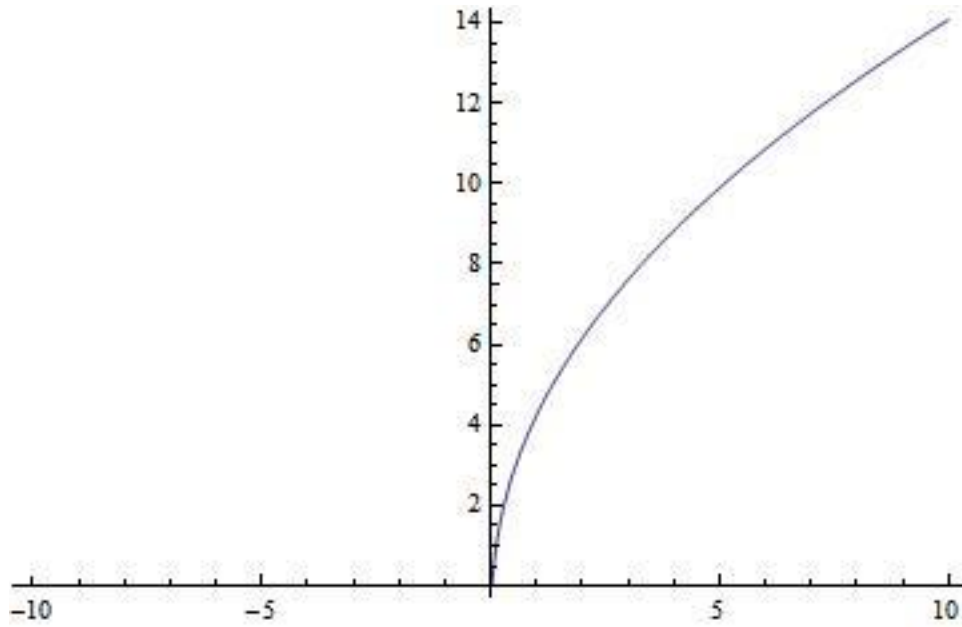
**Figure 7: Shape of the Magnetic Field strength vs Penetration Depth curve (positive) [9]**
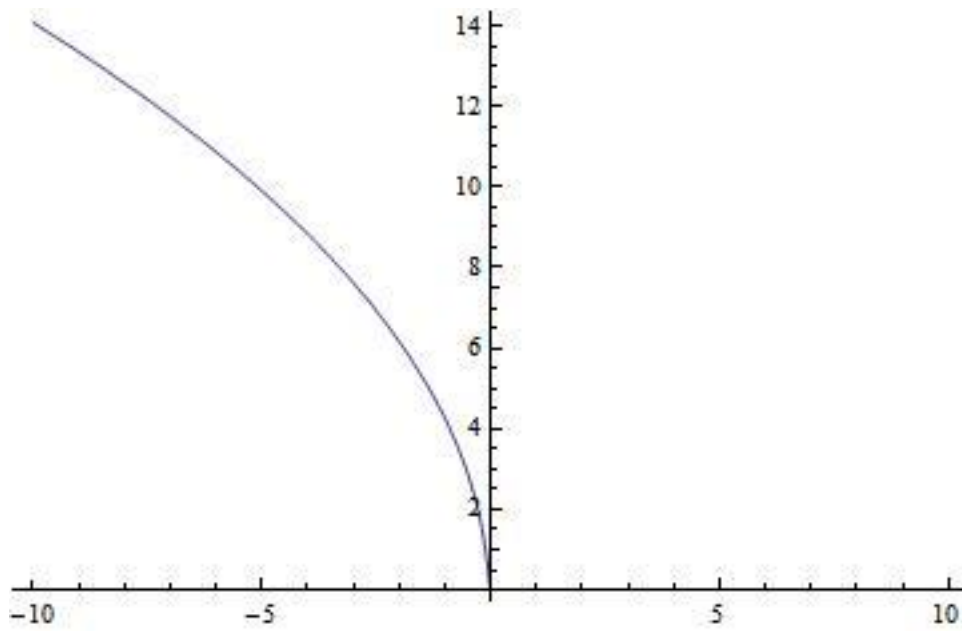


**Figure 8: Shape of the Magnetic Field strength vs Penetration Depth curve (negative) [9]**

Figures (9) and (10) show that the strength of the magnetic field in comparison to the London penetration depth diverges from the core of the magnetic flux vortex. At the vortex core as $r \to 0$, the magnetic field logarithmically diverges for the boundary condition of $(r \lesssim \xi)$ [13], [1]:

$$\boldsymbol{B}(0) \approx \frac{\Phi_0}{2\pi\lambda_L^2}\ln(\boldsymbol{\kappa}) \qquad \text{(eqn.3.2)}$$

Here $\left(\boldsymbol{\kappa} = \frac{\lambda_L}{\xi}\right)$ is the Ginzburg-Landau parameter classifying each type of superconductor based off of their respective penetration depths and superconducting coherence lengths [1]. These Vortices arrange themselves in a hexagonal *Flux-Line Lattice*, this lattice or FLL is an interpretation of a periodic solution to the Ginzburg-Landau equations by Abrikosov, describing periodicity of the magnetic flux properties of type-II superconductors along an established line of flux within the sample [6]. This line of pinned flux creates one quantum of magnetic flux $\Phi_{\boldsymbol{0}} = \frac{2\pi\hbar c}{2e_*} = 2.078 \; x \; 10^{-15} \; T \cdot m^2 \left(or \frac{kg \cdot m^2}{s^2 \cdot A^2}\right)$ created from the circulating flow of electron Cooper Pairs. The study of these "singularities" in the vortex lattice is at the forefront of research conducted pertaining to high-temperature superconductors.

The analysis of the supercurrent density is a very essential subject when exploring superconductivity, especially in thin film samples. But before the critical current density measurements can be made, a hysteresis curve of the magnetization in the (**a, b**) plane versus the auxiliary magnetic field **H** must be measured. This ensures that the thin film sample exhibits near perfect diamagnetism and will then have the persistent currents that arise in superconductors. Figure (11) shows this magnetization versus field measurement at 10K and then at 50K in figure (12).
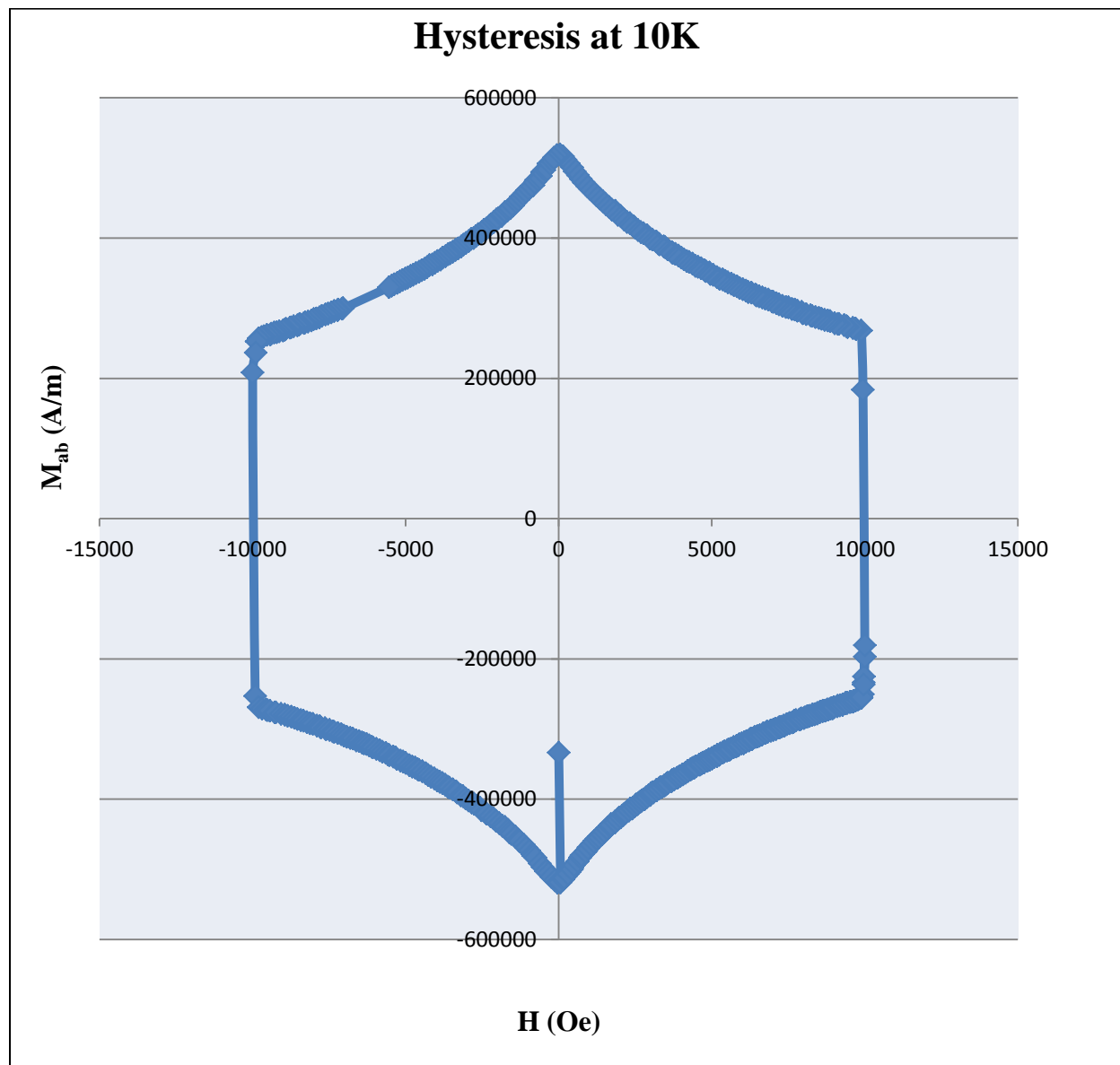
**Figure 9: Magnetization (M$_{ab}$) in the (a, b) plane as a function of the magnetic field (H)**
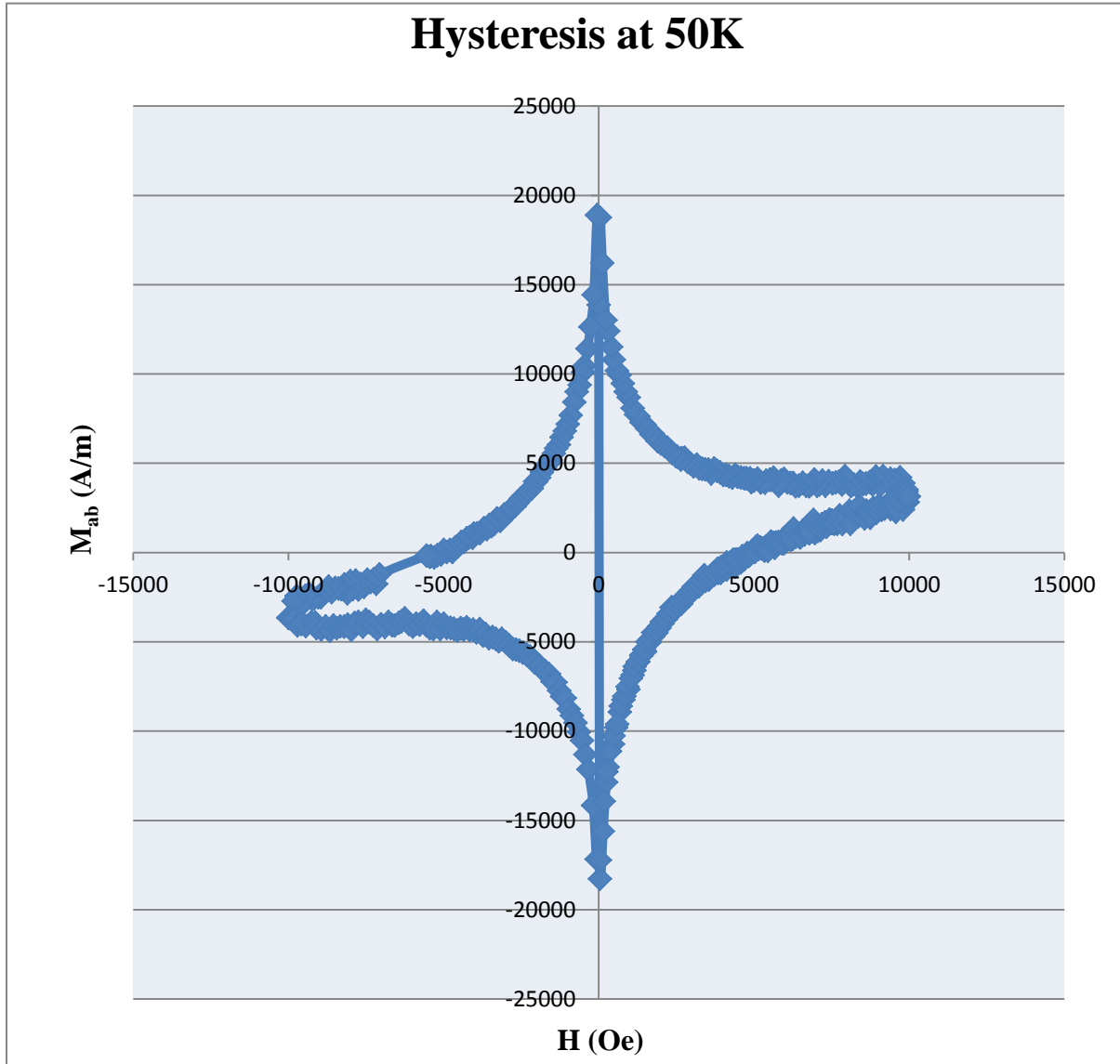
**Figure 10: Magnetization ($M_{ab}$) in the (a, b) plane as a function of the magnetic field (H)**

The abnormality in the hysteresis curve for the control sample at 50K in figure (12) is due to the proximity of the transition temperature (68.84K). This shows that the magnetization decreases and the so called *departing* of electron pairs begin to occur as the sample's temperature rises closer to the limit that is the transition temperature. This also suggests that the sample material did not have surface uniformity in terms of the deposition on to the substrate. Using the magnetization at 10K, the critical current density

can be calculated utilizing Bean's Critical State Model [14]. Figure (13) shows the critical current density versus the magnetic field **H** of the control YBCO thin film sample at 10K. These measurements of the, critical current density at 10K and magnetization at both 10K & 50K, provide a general basis on what to expect when creating YBCO thin samples. These measurements serve as reference for the theoretical framework of the electron pair velocity and their variation.



**Figure 11: Critical Current Density of YBCO control sample at 10K**

Further explaining the theory of the supercurrent density, here it is expressed in terms of the commutation of wave states:

$$J_s = e_* < \psi_* J_{op} \psi > = e_* \psi_* J_{op} \psi \qquad \text{(eqn.3.3)}$$

This accounts for the supercurrent density in the superconducting wave state with the charge of the paired electrons and the current de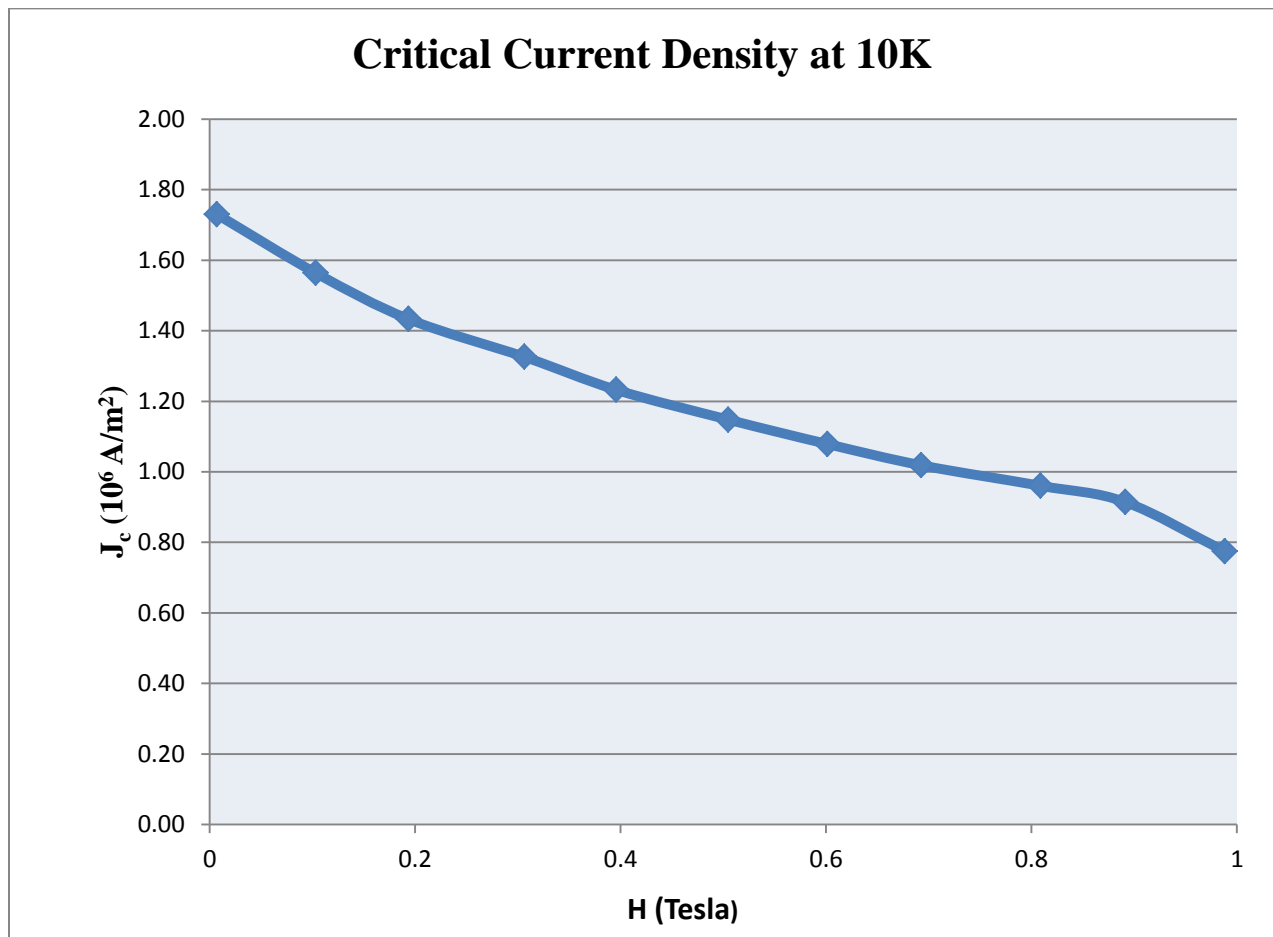nsity operation upon the wave states. Showing an exponential form of the order parameter $\psi(r)$ with amplitude $|\psi(r)|$, the supercurrent density takes on the expression in terms of the velocity of these paired electrons and the probability of the order parameter:

$$J_s = e_* |\psi|^2 \left( \frac{\hbar \nabla \phi}{m_*} \right) \qquad \text{(eqn.3.4)}$$

Where $\left( \frac{\hbar \nabla \phi}{m_*} \right)$ is the velocity of the paired electrons in energy state $\phi$ with electron pair mass $(m_*)$ and charge $(e_*)$ [9]. With the inclusion of the magnetic field effects on the current density the velocity of each pair is now formulated in terms of the magnetic vector potential and the potential energy of the state. Velocity of the paired electrons is in terms of the canonical momentum:

$$V_* = \frac{1}{m_*} \left( \hbar \nabla \phi - \frac{e_*}{c} A \right) \qquad \text{(eqn.3.5)}$$

Keeping both the electron pair mass and the reduced Planck constant in this expression for the velocity of the pairs suggests that the quantum mechanical operations for this coherent state is of a macroscopic nature. The expectation values, probabilities, and average densities are physical values and not just probabilistic.

Keeping focus on the fact that the pair mass term is still in this quantum mechanical expression for the velocity of paired electrons gives rise to the "inertial" dynamics of the pair themselves. This states that the critical current density of the pairs, and fundamentally the pair velocity, is reactive to some

external inertial force acting on the center of mass of the pair and the critical current density now becomes [9]:

$$J_* = \frac{e_* |\psi|^2}{m_*}\left(\hbar \nabla \phi - \frac{e_*}{c}A\right)$$

$$= \frac{e_* n_*}{m_*}\left(\hbar \nabla \phi - \frac{e_*}{c}A\right) \qquad \text{(eqn.3.6)}$$

The identification of the velocity of the paired electrons is important to this work due to the theoretical approach to understanding the supercurrent density and its properties relating it to the amount of force the paired electrons experience interacting with the Fluxon quasiparticle. A modification to this distribution of the supercurrent density from the doping of the superconducting samples due to the presence of nanodots suggests that the nanodots, normal zones of the lattice, exhibit a virtual work upon the paired electrons thus changing the supercurrent density. This increase to the current density by way of characterization of the normal state nanodots deposited onto the thin film sample, through laser deposition, will create a more stable system of paired electrons circulating these areas enclosing a single fluxon. The chemical potential and number density of the electron pair, fluxon and nanodots play a vital role in the source of the virtual work from the nanodots giving a relationship between the supercurrent density, the potential energy density created by the nanodot and the dynamics governing the thermodynamic properties of the lattice.

## 3.2  Temperature Dependence of Critical Current Density and Magnetic Flux

To modify the description of the temperature dependence of critical current density and the magnetic flux threading the superconductor in the presence of nanodots, a reformulation of the fundamental free-energy expression is needed.

$$dF = -SdT - \sum_k Q_k^{(r)} dr_k^{(r)} + \sum_j \mu_j dN_j \qquad \text{(eqn.3.7)}$$

Here the standard entropy and temperature terms hold for this thermodynamic state, $\sum(Q_k^{(r)} dr_k^{(r)})$ is the amount of virtual work from the nanodot interacting with the system of electron pairs. Recalling that the free-energy expression from the Ginzburg-Landau theory says:

$$F_{GL}(r) = F_{grad}(r) + F_L(|\Psi(r)|) + U_{mag}(B(r)) \qquad \text{(eqn.3.8)}$$

Utilizing the postulate of D'Alembert for virtual work on a system of particles and exploiting the notion that quantized magnetic flux lines can be treated as if they are quasiparticles called *Fluxon*, one can formulate a description of the free-energy interaction of these Fluxon with the supercurrent density surrounding them in terms of the chemical potential and nanodot number density. For the system acted upon by an external force or an interacting potential $(\chi_r)$,

$$\chi_r = -\frac{\partial E_r}{\partial x} \qquad \text{(eqn.3.9)}$$

The thermal average of this force is

$$\langle \chi \rangle = \sum_r P_r \chi_r = \left(\frac{1}{\beta}\right) \frac{\partial \log(z)}{\partial x} \qquad \text{(eqn.3.10)}$$

Suggesting the internal energy

$$dU = TdS - r_r d\chi_r + dF_{GL} \qquad \text{(eqn.3.11)}$$

From here an expression for the free-energy of the system can be derived using known theories pertaining to the Vortex state of superconductivity and free-energy thermodynamics [8]. The standard free-energy expression is stated:

$$dF = dU - SdT + \sum_i \mu_i dN_i \qquad \text{(eqn.3.12)}$$

If we include all interacting potentials involved in the system externally and internally then an expression for the free-energy is:

$$dF = \sum_r dU_r(\boldsymbol{r}_i) - SdT + \sum_i \mu_i dN_i + \mathbf{d}F_{GL} \qquad \text{(eqn.3.13)}$$

Solving this proposed free-energy description for the entire system of particles, including external interactions, for the chemical potential and number density could present a theoretical range for the number density of laser ablated nanodot nanodots. This solution could create a "tuning parameter" for high-temperature superconductivity generating a more efficient way of choosing an optimal impurity density. Another solution could arise from shifting the focus to the entropy of the system as it is related to the number of interacting particles within the system itself, further looking into why a pseudo-resistance occurs after a certain field limit has been reached from the activation energy induced by the fields.

# CHAPTER 4

## Tuning Parameters of the Superconducting State

### 4.1 Chemical Potential of the Normal-Superconducting State Interaction

Within the thermodynamic realm of the superconducting sample the chemical potential of all interacting particles and quasiparticles are important to consider. The number density of interacting particles and each of their chemical, or electro-chemical, potentials can alter the dynamics of the thermodynamic system. Since we are within a macroscopic quantum limit, the energy of the paired electrons is just simply their electro-chemical potential ($\mu_*$). If we consider all interactions that take place then the total chemical potential for the entire system (lattice, paired electrons, fluxon, and the magnetic influence) is:

$$\mu_{tot} = \sum_i \frac{\partial}{\partial N_i} \left[ \frac{1}{\beta} (\log(z) + \beta U_i) - \sum_k \boldsymbol{Q}_k^{(r)} d\boldsymbol{\chi}_k^{(r)} \right] + \sum_j \frac{\partial}{\partial N_j} [\phi_*] + \sum_k \frac{\partial}{\partial N_k} (\boldsymbol{m} \cdot \boldsymbol{B})$$

(eqn.4.1)

Here we can see that the total chemical potential of the entire system suggests that there are other quasiparticles at play interacting with the paired electrons comprising up the supercurrent. Simplifying this total chemical potential in equation (4.1) we have:

$$\mu_{tot} = \mu_k + \mu_*$$

(eqn. 4.2)

Where $\mu_k$ is the chemical potential of the nanodot and $\mu_* = \mu_e + e_* V_*$ is the electro-chemical potential for the electron pair in terms of the thermodynamic chemical potential of the pair and the usual electrostatic potential for charged particles.

Comparing this theory to the critical current density and nanodots density collected from a body of work with very similar YBCO thin film samples [8]:

Electron pair velocities can be calculated using the current density, collective charge of the superconducting pair and the number density of the superfluid (flow of paired electrons) [9], [11], [12]

$$v_* = \frac{J_*}{n_* e_*} \qquad \text{(eqn.4.3)}$$

**Table 2 Substrate Mod.:-TH-A (10 pulses), TH-B (30 pulses) Multilayer:-TH-A1 (10 pulses), TH-B1 (30 pulses)**

| Temperature | Samples | Current Density A/cm$^2$ | Pair Velocity cm/s |
|---|---|---|---|
| 5K | THA | 9.23E+07 | 3025689.656 |
| | THB | 6.65E+07 | 2179938.918 |
| | THA1 | 1.50E+07 | 491715.5455 |
| | THB1 | 2.35E+07 | 770354.3546 |

| Temperature | Samples | Current Density A/cm$^2$ | Pair Velocity cm/s |
|---|---|---|---|
| 77K | THA | 3.42E+06 | 112111.1444 |
| | THB | 3.78E+06 | 123912.3175 |
| | THA1 | 4.30E+05 | 14095.84564 |
| | THB1 | 6.00E+05 | 19668.62182 |

Considering the dimensions of the nanodots as $(\chi_\beta, \chi_\gamma)$, where these are the respective diameter (with $2\pi$ symmetry) and height of the nanodots, we can assume that the geometry of the nanodots follow that of a spheroid,

**Table 3 Substrate Mod.:-TH-A (10 pulses), TH-B (30 pulses) Multilayer:-TH-A1 (10 pulses), TH-B1 (30 pulses)**

| Samples | Nanodot Diameter $(\chi_\beta)$ | Nanodot Height $(\chi_\gamma)$ |
|---|---|---|
| THA/THA1 | 4.0-6.0nm | 1.7nm |
| THB/THB1 | 4.0-6.0nm | 4.0nm |

The average volume of each Cerium Oxide nanodots can be calculated using the following equation for a spheroid with $2\pi$ (**a, b**) plane symmetry,

$$V_{spheriod} = \frac{4}{3}\pi(a)^2 c$$

$$= \frac{4}{3}\pi \left(\frac{\bar{\chi}_\beta}{2}\right)^2 \bar{\chi}_\gamma \qquad\qquad \text{(eqn.4.4)}$$

**Table 4 Substrate Mod.:-TH-A (10 pulses), TH-B (30 pulses) Multilayer:-TH-A1 (10 pulses), TH-B1 (30 pulses)**

| Samples | Nanodot Radius $\left(\frac{\chi_\beta}{2}\right)$ | Volume of Nanodots |
|---|---|---|
| THA/THA1 | 2.0nm | 28.48377nm$^3$ |
| | 2.5nm | 44.50589nm$^3$ |
| | 3.0nm | 64.08849nm$^3$ |
| THB/THB1 | 2.0nm | 67.02064nm$^3$ |
| | 2.5nm | 107.71975nm$^3$ |
| | 3.0nm | 150.79644nm$^3$ |

Exploiting that Cerium Oxide with a mass density of $\sim 7.2148 \; x \; 10^{-22} g/nm^3$ We can calculate an approximate average mass of the nanodots based off of the density of Cerium Oxide and the average volume of the nanodots.

**Table 5 Calculated nanodots masses from the density of Cerium Oxide and their respective volume**

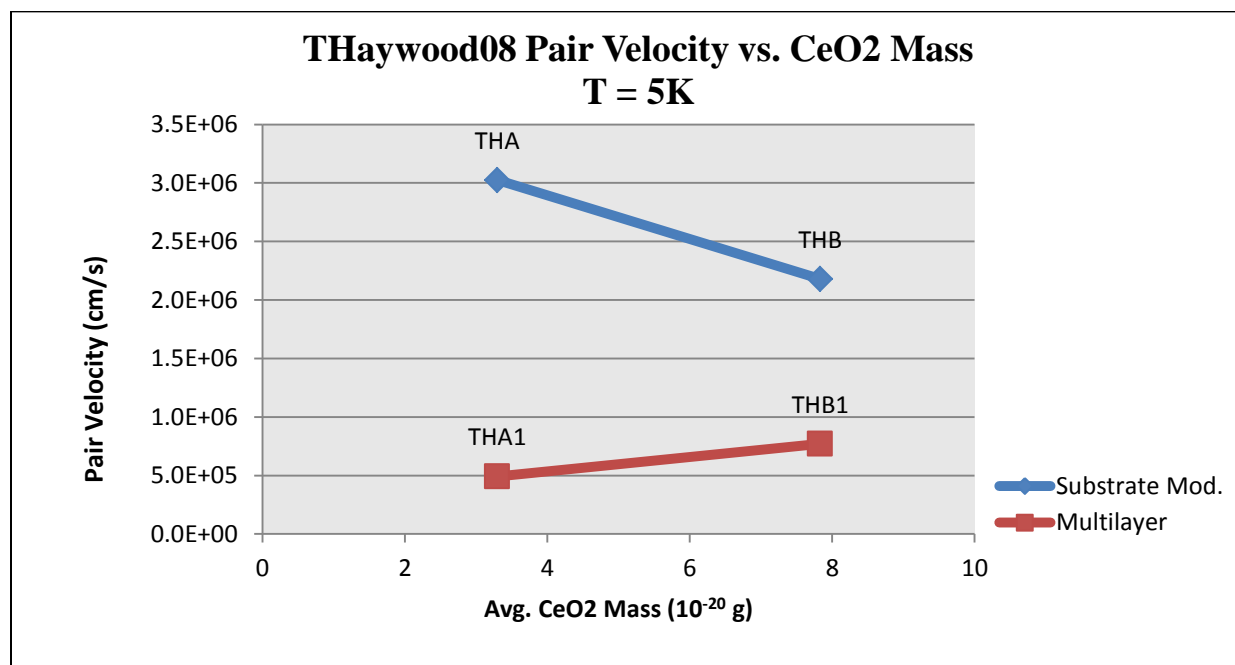| Nanodot Mass ($10^{-20}$ g) [10 pulses] | Nanodot Mass ($10^{-20}$ g) [30 pulses] |
|:---:|:---:|
| 2.055 | 4.83542 |
| 3.211 | 7.77179 |
| 4.624 | 10.87971 |
| (Average Mass) 3.29667 | (Average Mass) 7.82897 |



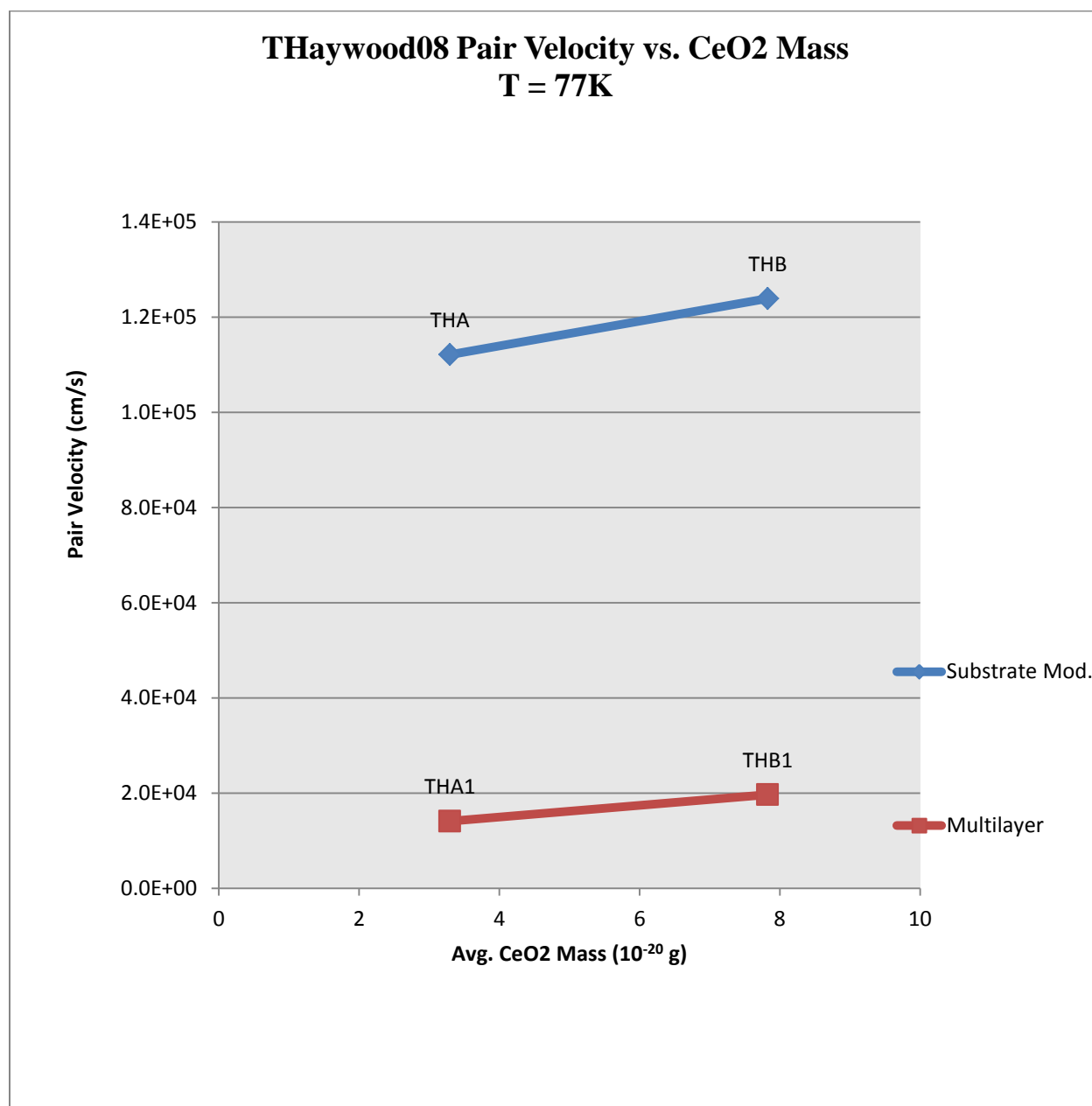Figure 12: Electron pair velocity correlation with average CeO$_2$ mass at 5K

**Figure 13: Electron pair velocity correlation with average CeO₂ mass at 77K**

## 4.2 Virtual Work by the CeO$_2$ Nanodot

Recall that there exists a total potential from the chemical potential of the Electron pair and the chemical potential of the modified lattice:

$$\mu_{tot} = \sum_i \frac{\partial}{\partial N_i}\left[\frac{1}{\beta}(\log(z) + \beta U_i) - \sum_k \boldsymbol{Q}_k^{(r)} d\boldsymbol{\chi}_k^{(r)}\right] + \sum_j \frac{\partial}{\partial N_j}(\phi_*) + \sum_k \frac{\partial}{\partial N_k}(\boldsymbol{m} \cdot \boldsymbol{B})$$

(eqn.4.5)

This total chemical potential simplifies to: $\mu_{tot} = \mu_* + \mu_k$, where [9], [3]

$$\mu_* = \mu_e + e_*V = -E \qquad\text{(eqn.4.6)}$$

and

$$\mu_k = \sum \frac{\partial}{\partial N}\left[\frac{1}{\beta}(\log(z) + \beta U) - \sum_k \boldsymbol{Q}_k^{(r)} d\boldsymbol{\chi}_k^{(r)}\right] \qquad\text{(eqn.4.7)}$$

Since the lattice structure of YBCO is periodic with respect to the electron pairs with temperature equal to zero, an approximation for the chemical potential $\mu_k$ governing the    anodots can be made in the form of the virtual work:

$$\mu_k = -\frac{\partial}{\partial N}\sum_k \boldsymbol{Q}_k^{(r)} d\boldsymbol{\chi}_k^{(r)} \qquad\text{(eqn.4.8)}$$

Equation (4.8) does not include the magnetic dipole moment and field due to the hole like behavior of the    anodots. Utilizing the virtual work from the perspective of the nanodots is not an obvious choice. From a very fundamental set of units describing magnetic flux, we can derive a relationship between virtual work and current density. The standard unit of measure for magnetic flux is normally a Weber (Wb) or a Tesla square meter $(T \cdot m^2)$, but we can further simplify these units in to even more fundamental ones.

$$Wb = T \cdot m^2 = \frac{Kg \cdot m^2}{s^2 \cdot A} \tag{eqn.4.9}$$

Now that the magnetic flux is recast in to units of length, mass, time, and current we can formulate a new equation describing the same physical action.

From the BCS theory the paired electrons have a velocity [9], [5], [8]:

$$\boldsymbol{v}_* = \frac{1}{m_*}\left(\hbar\nabla\phi - \frac{e_*}{c}\boldsymbol{A}\right) \tag{eqn.4.10}$$

With the inclusion of the mass, the paired electrons respond to an inertial force proportional to the acceleration [9]:

$$-\frac{\nabla\mu_*}{m_*} = \frac{d}{dt}[\boldsymbol{v}_*] \tag{eqn.4.11}$$

Exploiting that the electron pairs respond to an inertial force [9], [8], we see that it is obvious in these units that magnetic flux is merely the amount of work per current. A net force can be expressed from the interaction of the electron pair and the anodots:

$$\boldsymbol{F}_{*,net} = -\nabla(\mu_k + \mu_*),$$

$$+\nabla\mu_k = -\nabla\mu_*$$

$$= -\nabla\left(\boldsymbol{Q}_k^{(r)}d\boldsymbol{\chi}_k^{(r)}\right) + \left(-\nabla(\mu_e + e_*V)\right)$$

$$= -\nabla(\boldsymbol{Q}_k \cdot \boldsymbol{\xi}_*) + \left(-\nabla(\mu_e + e_*V)\right) \tag{eqn.4.12}$$

Here the virtual work is in an energy state ® operating within the momentum phase space of the system, and as usual the electrochemical potential arises for the electron pairs. Like all systems in equilibrium, this net force must equal to zero satisfying the conservation of energy and momentum of the interaction. Using this as motivation, we can express the magnetic flux as:

$$\Phi_k = \frac{(\boldsymbol{Q_k} \cdot \boldsymbol{\xi_*})}{J_* \cdot \left(\pi \left(\frac{\chi_\beta}{2}\right)^2\right)} + \Phi_0 \qquad \text{(eqn.4.13)}$$

Magnetic flux is in terms of the current density, an equivalent inertial force (a fictitious force) and the coherence length describing the size of the electron pairs related to the displacement the pairs should experience from the virtual work. As we can see here, $J_*$ is the respective supercurrent density of the sample at a specific temperature, $\pi \left(\frac{\chi_\beta}{2}\right)^2$ is the cross-sectional area of the nanodots keeping the radial symmetry of the geometry. While $\boldsymbol{\xi_*}$ is the characteristic superconducting coherence length, $\boldsymbol{Q_k}$ the fictitious force induced by the magnetic flux on a charged particle, and $\boldsymbol{\Phi_0}$ the quantum of magnetic flux (Fluxon), $2.0678 \; x \; 10^{-15} \; Wb$.

## 4.3 Electron Pair Velocity Variation

This *fictitious* force arises from the potential energy that the nanodot creates on the surface of the superconducting state in momentum space. Without the full use of an effective field theory only an approximation of the tuned velocity of paired electrons can be made.

$$\Phi_k = \frac{(\boldsymbol{Q_k} \cdot \boldsymbol{\xi_*})}{J_* \cdot \left(\pi \left(\frac{\chi_\beta}{2}\right)^2\right)} + \Phi_0$$

Using the basic physical laws that govern this interaction, the current density is [18]

$$\boldsymbol{J_*} = n_* e_* \boldsymbol{v_*} = \frac{I}{\pi r^2} \qquad \text{(eqn.4.14)}$$

For an approximation for a simple applied magnetic field $\boldsymbol{B}_a$ with magnetic flux $\Phi$ through an enclosed current carrying loop of radius $\boldsymbol{S}$, we can use the solution of [18]

$$\boldsymbol{\Phi} \approx \oiint (\boldsymbol{B}_a \cdot \hat{\boldsymbol{n}})\boldsymbol{ds} \approx \boldsymbol{B}_a \pi \boldsymbol{s}^2$$

$$\cong \boldsymbol{B}_a \pi \left(\frac{\chi_\beta}{2}\right)^2 \qquad \text{(eqn.4.15)}$$

From here we can solve for the current density and then the velocity of the electron pairs from with equation(6.13).

$$\boldsymbol{J}_* = \frac{\chi_\beta}{\Phi_k A}\left(-\nabla(\boldsymbol{Q}_k \cdot \xi_*)\right) + \boldsymbol{\Phi_0} \qquad \text{(eqn.4.16)}$$

$$\boldsymbol{J}_* \cong \frac{(\boldsymbol{Q}_k \cdot \xi_*)}{\boldsymbol{B}_a \pi \left(\frac{\chi_\beta}{2}\right)^2 \left(\pi\left(\frac{\chi_\beta}{2}\right)^2\right)} \qquad \text{(eqn.4.17)}$$

$$\boldsymbol{v}_* \approx \frac{(-\nabla(e_* v_* \boldsymbol{B}_a sin\phi) \cdot \xi_*)}{\pi^2 \left(\frac{\chi_\beta}{2}\right)^4 \cdot \boldsymbol{B}_a} \frac{1}{n_* e_*} \qquad \text{(eqn.4.18)}$$

Equation (4.18) makes this approximation in terms of the induced fictitious force portrayed by the Lorentz force. The electric field contribution is negligible due to the macroscopic electrodynamics explained through the London theory. This approximation gives a fairly wide range of percent difference $\%\text{diff} \approx (\sim 0.253 - 7.895) \, x \, 100\%$.
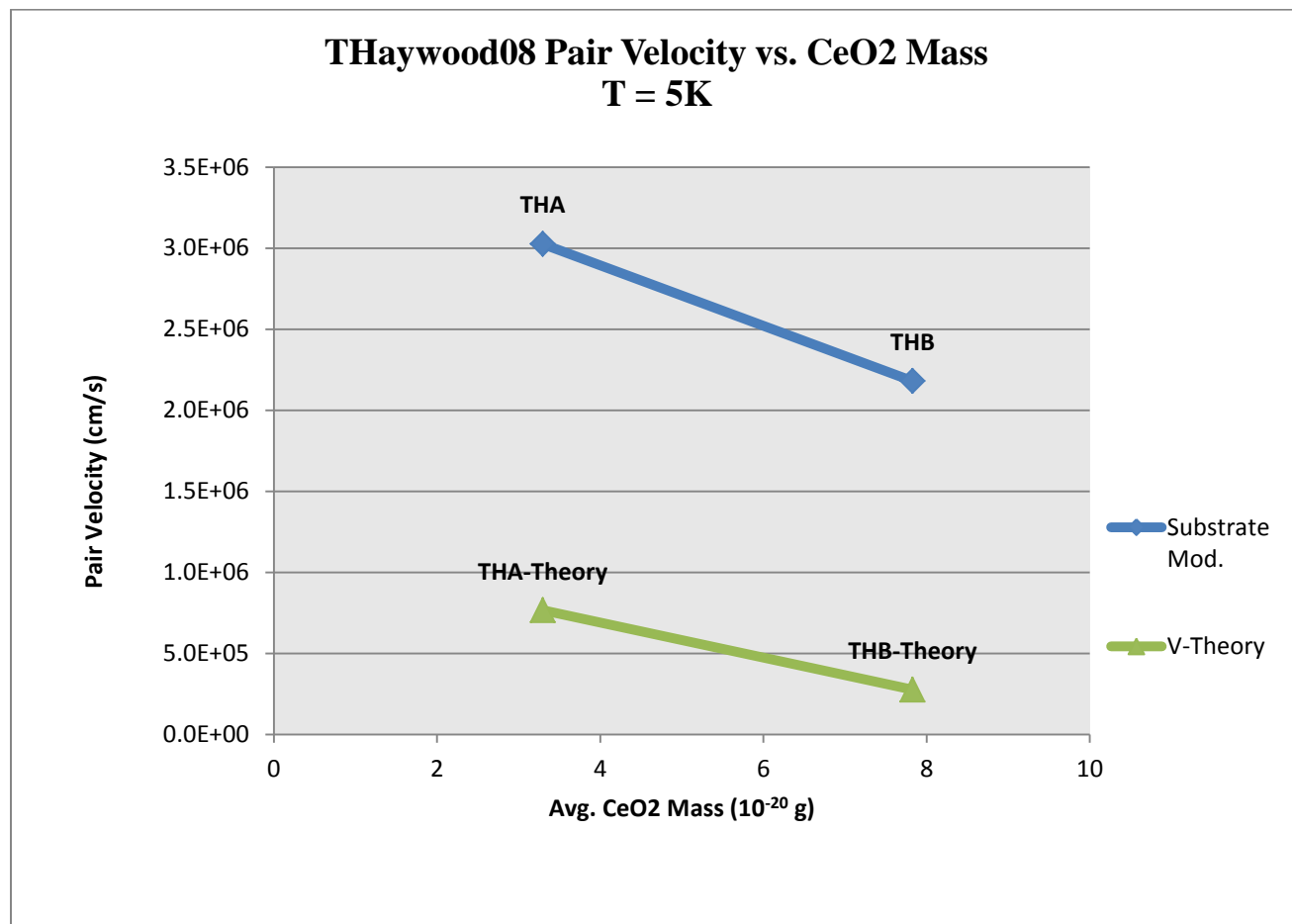
**Figure 14: Theoretical Electron pair velocity correlation with experimental data curve at 5K**
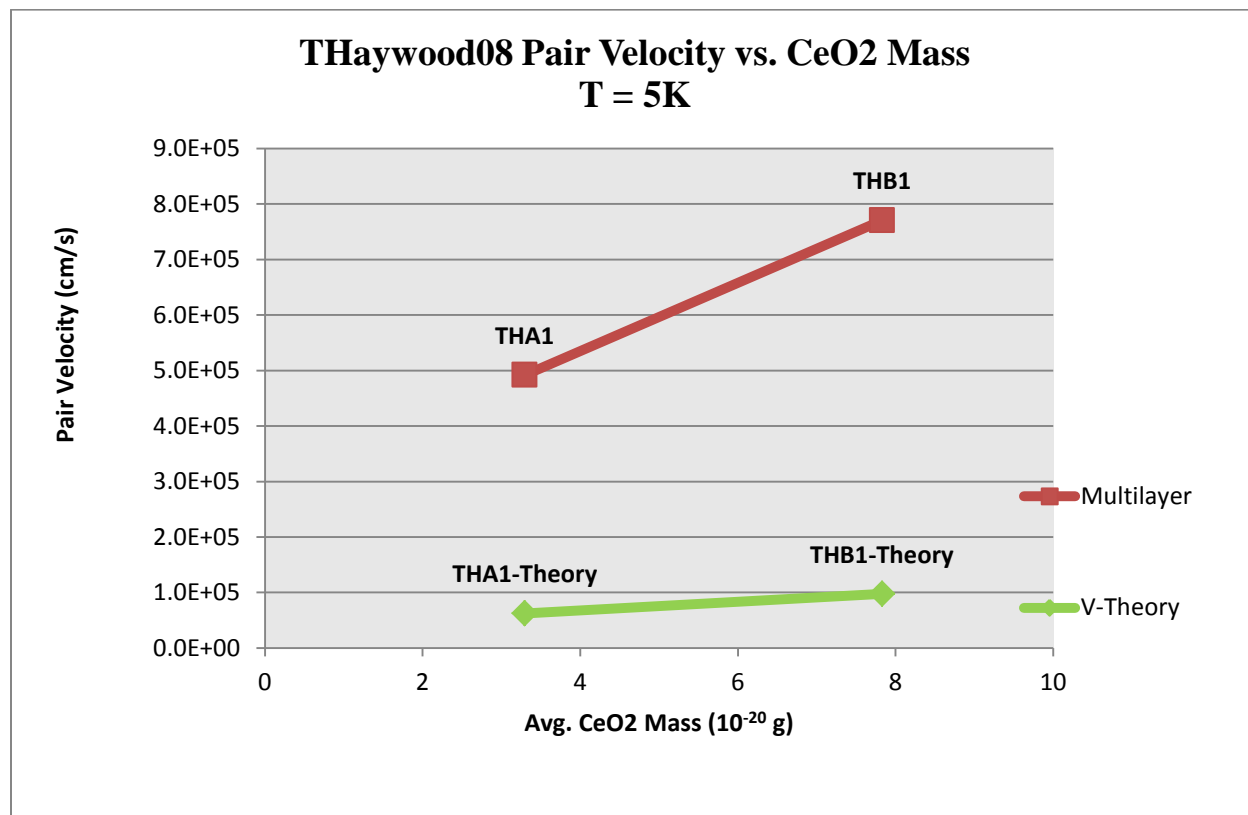
**Figure 15: Theoretical Electron pair velocity correlation with experimental data curve at 5K**

Figures (16) & (17) show that the theoretical values, closely equal in magnitude to the experimental values with some percent error, follow the same curve in terms of their data plots. The error in the 5K pair velocities is smaller than the 77K pair velocities due to the lack of any temperature dependence and due to the approximations that were made when calculating. We can see that there is a stronger relationship between the nanodots and the paired electrons in terms of their velocity. This suggests that theses magnetic flux vortices penetrating at the normal zones of the sample offer more than expected of them. These normal zones may offer an optimization to the superconducting sample instead of a defect in structure.

# CHAPTER 5

## Conclusion

Although this description of the variation of the superconducting electron pair velocity is incomplete, at the moment it shows promise in terms of further characterizing high-temperature superconductors. Characterization in terms of the respective nanodots densities and geometries seem very important to the critical current density. The chemical potential and virtual work from the thermodynamic energy states offer a step in the right direction to this characterization. Further correlating this description with known sources of experimental data, proven theories, and continued research on the subject matter will generate interesting insights to the study of theses magnetic singularities in high-temperature superconductors. Experimentally more data is needed from the measurements of the magnetization versus time, magnetization versus temperature, and direct measurements on the electron pair velocity. Looking in to the temperature dependence of the pair velocities, entropy, and possibly the pressure of the superfluid itself may deem worthy of more experimentation. The overall effective field theory governing this interaction is to be explored in greater detail, including the field parameters and recasting the model within the quantum mechanical limits.

To test these quantum mechanical parameters the utilization of SQUID (Superconducting Quantum Interference Device) technologies are needed to acquire precise measurements for proper use.

Future work will include completing this description including the Fermi energy and chemical potential based off of experimental data. X-ray Diffractometry, Scanning Electron Microscopy and nanodots characterization will be conducted. Creation of more samples with varied nanodot nanodots and the deposition of multiple nanodot species onto a single YBCO thin film will also be of interest.

# References

1. *Introduction to Solid State Physics.* **Kittle, Charles.** s.l. : J. Wiley & Sons, 2005.

2. *Introduction to Solid State Physics, London Equations.* **Kittel, Charles.** s.l. : Wiley & Sons, 2005.

3. *Superconductivity In Small Systems.* **Groff, Ronald.** s.l. : University of Rochester, 1967.

4. *Theory of Superconductivity.* **J. Bardeen, L. N. Cooper, and J. R. Schrieffer.** 1175, s.l. : Physical Review, 1957, Vol. 108.

5. *BCS Theory Lecture 7.3.* **Henley, Christopher L.** Ithica, NY : Cornell University, 2009.

6. *Phase diagram of the t–U2 Hamiltonian of the weak Coupling Hubbard Model.* **Yanagisawa, Takashi.** s.l. : New Journal of Physics, 2008.

7. *On The Theory of High-Temperature Superconductivity: from Electronic Structure to Fluctual Properties and Electrodynamic Behavior.* **Mishonov, Todor Mihaylov.** s.l. : University of Sofia, 2007.

8. *Highlights of Macroscopic Superconductivity, 6.1.* **Henley, Christopher.** Ithica, NY : Cornell University, 2010.

9. *ICMR School on Novel Superconductors: Notes on the Ginzburg-Landau Theory.* **Beasley, M.R.** s.l. : University of California, Santa Barbara, 2009.

10. *Fabrication of YBCO Thin Films by Pusled Laser Deposition Technique and their Characteristics.* **TOZAN, Şerife.** s.l. : Izmir, 2010.

11. *Structural and Flux-Pinning Properties of Laser Ablated YBa2Cu3O7 Thin Films: Effects of Self-Assembled CeO2 Nanodots on LaAlO3 Substrates.* **Talisha Haywood, Sang Ho Ohb, Abebe Kebede, Devdas M. Pai, Jag Sankar, David K. Christen,Stephen J. Pennycook, Dhananjay Kumar.** s.l. : Physica C, 2008.

12. *Anomalous asymmetry of the Fermi surface in the YBa2Cu4O8 high temperature superconductor revealed by Angle Resolved Photoemission Spectroscopy.* **Takeshi Kondo, R. Khasanov, Y. Sassa, A. Bendounan, S. Pailhes, J. Chang, J. Mesot.** s.l. : Physical arXiv, 2013.

13. *On Abrikosov Lattice Solutions of the Ginzburg-Landau Equations.* **T. Tzaneteas, I.M.Sigal.** s.l. : arXiv, December 2011. 1112.1897.

14. *Irreversible magnetization in thin Y BCO films rotated in external Magnetic Field.* **R. Prozorov, A. Poddar, E. Sheriff, A. Shaulov, Y. Yeshurun.** Institute for Superconductivity, Physics Department, Bar-Ilan University, : Physical arXiv, 1996. arXiv:supr-con/9605001.

15. *Interaction of Superconductor Quantum Fluid.* **Desbrandes, Robert.** Baton Rouge, LA : Louisiana State University.

16. *Pinning effects on the vortex critical velocity in type-II superconducting thin films.* **A. Leo, G. Grimaldi, A. Nigro a, S. Pace , N. Verellen, A.V. Silhanek, W. Gillijns, V.V. Moshchalkov,.** s.l. : Physica C, 2010.

17. *Hydrodynamics of liquids of arbitrarily curved flux-lines and vortex loops.* **Panayotis Benetatos, M. Cristina Marchetti.** Syracuse, NY : Syracuse University, 2013.

18. *Classical Electrodynamics.* **J.Jackson.** s.l. : Wiley, 1998.